Most reactions yield cross sections whose values are fairly independent of the mass of the target. However, the values of the (p,pn)-reaction cross sections vary quite a bit as the target mass is changed. Much of this variation appears to be due to differences in the number of available neutrons in the various target nuclei (Table II). In another paper an attempt will be made to describe the magnitude and variation of the (p,pn)-reaction cross sections.

VI. ACKNOWLEDGMENTS

I want to express my gratitude to Professor I. Perlman under whose supervision this work was done. My thanks are also extended to Dr. M. Kalkstein who performed one of the Na^{22} analyses and helped with a few other bombardments. I am grateful to Dr. Lester Winsberg and Dr. John Alexander for many helpful discussions. I appreciate the assistance with the target bombardments given by Dr. E. Lofgren and the Bevatron operating crew.

PHYSICAL REVIEW VOLUME 119, NUMBER 1 JULY 1, 1960

Nuclear Structure and Simple Nuclear Reactions*†

PAUL A. BENIOFF‡
Lawrence Radiation Laboratory, University of California, Berkeley, California
(Received December 18, 1959; revised manuscript received March 9, 1960)

Recently it has become increasingly evident that some assumptions in the nuclear model used for the Monte Carlo calculations yield cross section values which are not in accord with experiment. In particular, calculations of (p,pn)-reaction cross sections in the Bev energy range give values which are low by factors of two to nine when compared to experimental values. The calculated cross sections also show a smooth variation with the target atomic weight whereas the experimental values show quite an erratic variation. Reasons which have been advanced to account for this lack of agreement are the lack of a nuclear surface and failure to account for shell effects in the nuclear model used.

In this work a theory is developed to take account of surface and shell effects and thereby describe the observed magnitude and variation of the cross sections for simple nuclear reactions as exemplified by the (p,pn) reaction. At multi-Bev energies to which this treatment is restricted, the main contribution to the (p,pn)-reaction cross section comes from inelastic collisions between the incident protons and target neutrons, with all the p-n collision products escaping without further interaction. Approximations and assumptions used include the impulse approximation, 0° lab scattering angle for the inelastic p-n collision products, classical trajectories for the incident and scattered particles, and a quantum-mechanical treatment for the target nucleons. The multi-Bev, n-p, cloud-chamber data was used to determine the average total exit cross section for the inelastically scattered particles. The only neutron shells in the target nucleus contributing to the (p,pn) reaction are those for which the instantaneous knocking out of a neutron creates a product-neutron hole state stable to particle emission. The combination of these assumptions gives integral expressions which, when evaluated on the IBM-701 computer for the independent particle harmonic-oscillator shell model, give the (p,pn) reaction cross sections as a function of the nuclear density distribution and the number of available shells.

For the low Z nuclei where the available shells can be unambiguously determined, the results give a half-central-density radius parameter, r_0, ($r_0=R_{\frac{1}{2}}/A^{\frac{1}{3}}$), of about 1.2 fermis compared to 1.03 fermis for the charge half radius from the electron-scattering work. Use of reasonable limits on the value of r_0 allows one to set the minimum number of shells available for some targets. For example, the Zn^{64}, Cu^{65}, and Cu^{63} (p,pn) cross sections require that a large part or all the $1f_{7/2}$ neutrons be available, or, equivalently, that a $1f_{7/2}$ neutron hole state (across a major shell) in the product nucleus have less than 8- to 9-Mev excitation energy. The results also show that the energy associated with nuclear rearrangement to particle-stable product states must be less than 8 to 9 Mev. In several cases, the upper limit can be lowered considerably (to 1.5 Mev and 0 Mev in the cases of O^{16} and N^{14}, respectively).

I. INTRODUCTION

IN recent years a large number of cross sections for various types of spallation reactions has accumulated.[1–7] The Monte Carlo method[8,9] coupled with a Fermi gas model of the nucleus has been used to interpret the experimental results. At medium and

* This work was performed under the auspices of the U. S. Atomic Energy Commission.

† Present address: Department of Nuclear Science, Weizmann Institute of Science, Rehovoth, Israel.

‡ Submitted in partial satisfaction of the requirements for a Ph.D. degree at the University of California, Berkeley, California.

[1] Paul A. Benioff, preceding paper [Phys. Rev. **119**, 316 (1960)].

[2] Donald Barr, thesis, University of California Radiation Laboratory Report UCRL-3793, May, 1957 (unpublished).

[3] W. E. Burcham, J. L. Symonds, and J. D. Young, Proc. Phys. Soc. (London) **A68**, 1001 (1955); J. L. Symonds, J. Warren, and J. D. Young, Proc. Phys. Soc. (London) **A70**, 824 (1957).

[4] S. S. Markowitz, F. S. Rowland, and G. Friedlander, Phys. Rev. **112**, 1295 (1959).

[5] David R. Nethaway and Lester Winsberg, University of California Radiation Laboratory Report UCRL-8908, December, 1959. Phys. Rev. (to be published).

[6] I. M. Ladenbauer and L. Winsberg, University of California Radiation Laboratory Report UCRL-8907, October, 1959 (unpublished).

[7] Gösta Rudstam, thesis, Uppsala, Sweden, 1956 (unpublished).

[8] M. Goldberger, Phys. Rev. **74**, 1269 (1958).

[9] N. Metropolis, R. Bivins, M. Storm, A. Turkevich, J. M. Miller, and G. Friedlander, Phys. Rev. **110**, 185 (1958); **110**, 204 (1958).

high bombarding energies (hundreds of Mev and up) and for products whose mass is more than a very few atomic mass units less than that of the target, the existing calculations are in fair agreement with the experimental results.[2,9] However, for (p,pn) and $(p,2p)$ reaction products whose mass is one unit less than that of the target, the calculated cross sections, when compared to experimental values, are low by a factor of two to nine.[2,4,9,10] Also the calculations predict a smooth dependence of the cross section with the atomic mass of the target, whereas the experimental p,pn and $p,2p$ cross sections show quite an erratic variation. It has been suggested that adding a diffuse nuclear boundary to the existing Monte-Carlo calculations would correct this discrepancy.[9] Possible shell-structure effects have been advanced as an explanation for the apparent irregularity in the experimental values,[1,3,4]

Because of the existing discrepancy it was thought worthwhile to try a method of calculating cross sections based on the optical and shell models with a diffuse nuclear surface. In this work simple nuclear reactions include the (p,pn); $(p,2p)$; $(p,p\pi^-)$ [including (p,n)]; $(p,p\pi^+)$, and (p,p') reactions. This work will be restricted mainly to (p,pn) reactions because of the relative preponderance of (p,pn) reaction cross section data in the literature. However, with minor changes the results apply just as well to the other reactions mentioned.

The reaction mechanism that will be treated here in detail is that in which an incident nucleon makes a single collision with a target nucleon in a nucleus and all the fast collision particles leave the nucleus without further interaction. In order that this be the main mechanism contributing to the cross sections of the simple nuclear reactions, this work must be restricted to high incident energies (hundreds of Mev and up) so that nucleon evaporation by the nucleus will make a negligible contribution to the reaction cross sections. This reaction mechanism is applied to the reactions given above by requiring that the struck nucleon be in a shell whose distance below the topmost occupied level is less than the binding energy of the least bound particle in the product nucleus.

In order to make actual calculations the incident and exit particles will be assumed to have classical trajectories throughout the nucleus. Also, the fast particles produced by the inelastic fraction of the nucleon-nucleon collisions will be assumed to be moving in the same direction as the incident nucleon (zero degree lab scattering angles). Since this latter assumption is definitely invalid for elastic nucleon-nucleon collisions, the theory will be restricted further to the multi-Bev bombarding energy region where the fraction of the total nucleon collision cross section which is elastic is small. The restriction to the multi-Bev energy region also improves the zero degree lab scattering angle and classical trajectory approximations and the validity of the neglect of nuclear evaporation as a contributing reaction mechanism.

For the same reaction mechanism as that given above, Maris *et al.*[11] derived an expression for the differential $(p,2p)$ reaction cross section based on the theory of direct interactions. They made a rough estimate of the effect of multiple collisions in the nucleus on the reduction of the differential p-p scattering cross section. They showed that this effect reduced the cross sections by a large factor which increased with increasing target atomic weight and decreasing bombarding energy. Since they were considering proton energies within a small energy region and the reduction by multiple collisions is spread out over the whole energy region, the large reduction factors did not destroy the peaks in the proton energy spectra.

In the present work, the multiple collision reduction factor would also be expected to be large due to the dominance of multiple pion production in nucleon-nucleon collisions. However, only total reaction cross sections are considered so that the integrated energy spectrum of the scattered particles over the whole region is used. Consequently, the large reduction factors apply directly to the reaction cross sections and must be determined more accurately.

In Secs. II A–D the various approximations on which this work is based are given. The impulse approximation and use of classical trajectories are discussed in Sec. A. In B the validity of the zero degree lab scattering angle approximation is investigated by looking at the angular intensity spectrum of inelastic and elastic Bev nucleon-nucleon collisions. It is shown that this approximation is pretty good for high-energy inelastic nucleon-nucleon collisions and is invalid for elastic collisions.

In Sec. III the various p,pn reaction mechanisms are discussed. Again the multi-Bev n-p and p-p cloud chamber data is used to show that single p-n collisions followed by escape of the collision particles are the main contributors to that part of the p,pn reaction cross section coming from inelastic p-n collisions. Grazing inelastic p-n or p-p collisions followed by evaporation of a neutron contribute $<5\%$ of the contribution of the above mechanism.

The equations giving the (p,pn) [and $(p,2p)$] reaction cross sections are derived in Secs. IV A–E and the results of machine integration of the final equations are given. Section A develops the theory for inelastic single collision processes. The final result, Eq. (10), is an expression for M_{nlj}, the probability per target neutron in the nlj shell for single collision processes of the type already discussed. The harmonic oscillator nuclear model was put into Eq. (10) to give Eq. (13).

[10] A. Caretto and G. Friedlander, Phys. Rev. **110**, 1169 (1958).

[11] H. Tyrén, P. Hillman, and Th. A. J. Maris, Nuclear Phys. **7**, 1 (1958); **7**, 10 (1958); Th. A. J. Maris, Nuclear Phys. **9**, 577 (1958).

Section B outlines the IBM-701 integration of Eq. (13). Section C describes contour plots of the r,z integrand of Eq. (13) obtained from the machine. It is shown there that most of the single collision processes tend to occur in the nuclear surface and on the downbeam side of the nucleus. The final results of the machine integration of Eq. (13) are described in Sec. D and plots of M_{nl} for different values of n and l, the target atomic weight, and the spring constant are given. Useful relations, Eqs. (18a–c), for interpolating to values of M_{nl} for different values of the three input parameters than those used are given. In Sec. E the contribution to the p,pn reaction cross section for elastic p-n collisions is estimated in terms of a factor, F, which gives the probability of escape from the nucleus of the struck neutron. Eq. (21) is the final result of these calculations and gives the p,pn cross section in terms of the various parameters discussed above.

Before Eq. (21) can be applied to nuclei, the various parameters appearing have to be evaluated and some general properties of the results discussed. This is done in Secs. V A–E. The evaluation of $\bar{\sigma}$ from 3.4-Bev n-p cloud chamber data is discussed in Sec. A. The Pauli Principle and meson absorption are included in the final value of $\bar{\sigma}=168$ mb. The elastic-collision neutron-escape factor, F, is roughly estimated in Sec. B to be 0.5. Upper and lower limits of $0.1<F<0.9$ corresponding to a perfectly black and transparent nucleus, respectively, are set. It is shown in the next section that the errors contributed to Eqs. (22) and (23) by requiring F to lie within the reasonable arbitrary limits, 0.25 and 0.75, are smaller in most cases than the experimental error limit on the (p,pn) reaction cross section. The remaining factors in Eq. (21) are given in Sec. C and combined into Eqs. (22) and (23) which are the final results of all the previous discussion and are to be applied to 5.7- and 3.0-Bev (p,pn) reaction cross-section data, respectively. Equation (22) is

$$\sigma_{ppn}=(34\pm2)\sum_{\substack{\text{allowed}\\ \text{shells}}}N_{nlj}M_{nl},$$

where σ_{ppn} equals the ppn reaction cross section in mb. The constant in the brackets represents the evaluation of the factors appearing before the summation sign in Eq. (21) and is roughly equal to the total p-n collision cross section. The summation is over the n,l,j shells for which the sudden removal of a neutron leaves the product nucleus in an excited state stable to particle emission. The number of neutrons in the n,l,j shell is given by N_{nlj}. The probability per neutron that the incident nucleon collides with an n,l neutron and all the collision products escape without further interaction is given by M_{nl}. The j quantum number does not appear on M_{nl} because of the j degeneracy of the wave functions for the independent-particle harmonic-oscillator model which was used in Eq. (13) ff. It should be stressed though, that Eq. (10) is more general and holds for any potential well shape. Eqs. (16), (18a) and Figs. 3 and 4 are used with Eq. (22) to give $\sigma_{p,pn}$ as a function of allowed shells and the nuclear half density radius parameter, r_0.

Section V D discusses the reasons why this theory satisfies the important requirement that $\sigma_{p,pn}$ be independent of the bombarding energy in the Bev energy region. Section E cautions against taking Eqs. (21) to (23) too literally. They were derived on the basis of an independent particle model of the nucleus whereas real nuclei consist of interacting nucleons. Several errors introduced by neglect of nucleon-nucleon coupling are discussed.

The results of comparison of theory with experiment are discussed in Secs. VI A–E. Equations (22) or (23), (16) and (18a) and Figs. 3 and 4 give $\sigma_{p,pn}$ as a function of the allowed shells and the half density radius parameter. In Sec. A the shell spacings are taken from the calculations of Ross, Mark, and Lawson[12] and combined with binding energies to determine the allowed shells. Values of r_0 are then computed from all the experimental values of $\sigma_{p,pn}$ available and are compared mainly with values of the half-charge density r_0's given by electron scattering. The agreement on the whole is quite satisfactory. The value of $\sigma_{p,pn}$ for C^{12}, N^{14}, and O^{16} provide a more critical test of the theory as several approximations made, are exact for these nuclei. Both the allowed shells and r_0 are taken as unknowns in Sec. B and, using the experimental values of $\sigma_{p,pn}$, r_0 is given as a function of the allowed shells. It is shown that for some cases a minimum number of available shells can be set using the requirement that r_0 be within a reasonable range of values. When combined with neutron binding energies this allows one to set upper limits on the spacing of the upper shells. For example it is shown that for Cu^{65} and Zn^{64} the $1f_{7/2}$-$1f_{5/2}$ neutron shell spacing must be less than 8 Mev. Section C discusses the large disagreement between the r_0 values given for the Ce^{142} nucleus and the electron scattering r_0's. An interesting consequence of the initial approximations made (Sec. II) is discussed in Sec. D. It is shown that the rearrangement energy associated with the nuclear rearrangement coming from the snatching out of a target neutron must be less than 8 Mev most of the time. The lowering of this upper limit to 0 Mev, 0.68 Mev and $\ll$8 Mev for N^{14}, O^{16}, and Zn^{64}, respectively, is discussed. In Sec. E other possible uses of the p,pn cross sections are discussed.

Section VII discusses some possible error sources implicit in the approximations made which are difficult to evaluate at present. Section VIII concludes the main body of the work.

The three appendices give mathematical derivations

[12] A. A. Ross, H. Mark, and R. D. Lawson, Phys. Rev. **102**, 1613 (1956); the legends on Figs. 1 and 4 are interchanged in this reference. R. Lawson, Enrico Fermi Institute of Nuclear Studies, Chicago, Illinois (private communication).

the results of which were needed in the text at various points. Appendix I gives several equations describing relativistic p-n elastic scattering. Appendix II gives the derivation of Eq. (16) on the basis of the Thomas-Fermi model of the nucleus. The accuracy of Eq. (16) is found by comparing the values of r_0 obtained from the actual sum-over-squared wave functions to those obtained from Eq. (16). In Appendix III Eq. (10) is integrated analytically for the uniform density model, the one used in all the Monte Carlo calculations made to date. The values of $\sigma_{p,pn}$ calculated for Cu^{64} and Ce^{140} at 3 Bev are slightly lower than the actual Monte Carlo values obtained at 1.8 Bev but are within the error limits given on the Monte Carlo results.

II. APPROXIMATIONS

A. Impulse Approximation

At high incident energies the impulse approximation should be valid[13]; i.e., the wavelength of the incident proton is sufficiently short that the proton may be considered to interact with only one nucleon at a time in the nucleus. The effect of the rest of the nucleons is to provide a potential well and a resultant momentum distribution for the particular target nucleon considered. Also the time it takes for the incident nucleon to enter the nucleus and collide with a target nucleon and for the elementary collision products to leave is so short that the nucleus would not have time to rearrange itself or affect the course of the elementary collision. The exclusion principle has a small effect on the elementary nucleon-nucleon collision, as the amount of momentum space forbidden is small compared to the volume available. The incident proton can then be considered to have "snatched" a nucleon from the nucleus so fast that the only effect is to leave the target nucleus in any one of several excited nucleon-hole states.[14] If the products of the elementary collision get out of the nucleus without further interaction, and the particular resultant excited state of the nucleus is not a particle-emitting state, the product nucleus contributes to the (p,pn) or $(p,2p)$ cross section.

B. Zero-Degree Scattering-Angle Approximation

Another approximation which greatly simplifies the calculations is that, for inelastic n-p and p-p collisions, the particles are scattered at zero degrees in the laboratory system. The validity of this approximation can be seen from an examination of the free n-p collision data. Cloud-chamber data taken for 1.72-Bev average-energy neutrons on hydrogen[15] show that all the doubly produced mesons have a median laboratory scattering angle of 41 degrees (deg). The nucleons associated with these mesons have a median laboratory scattering angle of 17 deg. Singly produced mesons and the associated nucleons have median laboratory scattering angles of 34 deg and 20 deg, respectively. Inelastic events produced by 3.8-Bev average-energy neutrons on hydrogen[16] show that one half the particles are emitted within 20 deg (lab) of the primary beam, and two thirds within 30 deg of the primary beam. Roughly one-half of the inelastic events emit all particles within 35 deg of the forward direction, and there are only a few events which emit two or more particles at an angle greater than 35 deg. Three-fourths of the charged particles produced by 5.3-Bev p-p collisions emerge within 20 deg of the incident beam.[17] Other work indicates a median laboratory scattering angle of 32 deg for neutral pions produced by 6.2-Bev proton-nucleon collisions.[18] Cosmic-ray work indicates that for higher incident energies, the median laboratory scattering angle is as small as, or smaller than, the values given above.[19,20]

Contrary to the case for inelastic collisions, the approximation of a zero-degree scattering angle for the products is definitely invalid for n-p and p-p elastic collisions. The $\cos^n\theta$ angular dependence [taken to be the same in the forward center-of-mass (c.m.) hemisphere for p-n as for p-p collisions, (Appendix I)] ensures that at high energies ($n \gg 1$) either one or the other of the nucleons has a very high probability of being scattered at large angles (close to 90 deg) and having a low energy in the laboratory system.[21,22] At 5.7 Bev, the energy and scattering angle of the target particle in the laboratory system corresponding to the angle in the c.m. system at which most nucleons are emitted (the maximum of $\cos^n\theta \sin\theta$ where $n=36$) is 39 Mev and 80 deg (Appendix I). The same cosine dependence of the scattering angle ensures that the other nucleon is scattered at almost zero degrees in the laboratory system.

The invalidity of the zero-degree laboratory scattering-angle approximation for elastic p-n and p-p collisions is one of the reasons the ensuing treatment is restricted to multi-Bev bombarding energies where the elastic fraction of the total collision cross section is low. Because the contribution to the p,pn cross section from elastic p-n collisions can be only crudely estimated, restriction of the bombarding energy to the multi-Bev region minimizes the error in this estimation.

[13] Geoffrey Chew, Phys. Rev. **80**, 196 (1950).
[14] W. Selove, Phys. Rev. **101**, 231 (1956).
[15] W. B. Fowler, R. P. Shutt, A. M. Thorndike, and W. L. Whittemore, Phys. Rev. **95**, 1026 (1954).
[16] Fred Holmquist, thesis, University of California Radiation Laboratory Report UCRL-8559, December, 1958 (unpublished). The author also wishes to thank Dr. Holmquist for providing unpublished data.
[17] Wilson Powell, Lawrence Radiation Laboratory (private communication).
[18] D. King. Phys. Rev. **109**, 1344 (1958).
[19] N. Duller and W. Walker, Phys. Rev. **93**, 215 (1954).
[20] G. Bernardini, E. T. Booth, and S. J. Lindenbaum, Phys. Rev. **85**, 826 (1952).
[21] B. Cork, W. A. Wenzel, and C. W. Causey, Phys. Rev. **107**, 859 (1957).
[22] Lester Winsberg, Lawrence Radiation Laboratory (private communication).

C. Use of Classical Trajectories

Another helpful approximation depends on the fact that at Bev energies the wavelength of the incident nucleon is small compared to nuclear dimensions (λ is 0.03 fermi for a 6-Bev nucleon). Consequently, the incident nucleon may be considered to have a classical trajectory in the nucleus. The particles scattered in the inelastic p-n or p-p collision in the nucleus will also be assumed to have classical trajectories (λ is 1.1 and 0.4 fermis for 100-Mev pions and nucleons, respectively).[8] On the other hand, all the target nucleons have insufficient momentum, especially in the surface region, to be treated classically and will be treated quantum mechanically.

D. Other Approximations

The use in this work of the high-energy cloud-chamber scatter-diagram data depends on the assumption that the energy and angular distributions of the scattered particles for free n-p collisions can be "inverted" to describe p-n collisions and then lifted into the nucleus with, at most, small resultant changes. The inversion can be accomplished by exchanging the forward c.m. hemisphere for the backward c.m. hemisphere. The angular and energy distributions of the scattered particles in the nucleus will be affected by a number of factors such as the Pauli exclusion principle, motion of the target nucleon, etc. It will be shown later that most of the contributions to the (p,pn) reaction come from the nuclear surface where the effect of these factors is small.

III. (p,pn) REACTION PATHS

A consideration of (p,pn) reactions indicates that there are several possible paths by which a product containing one neutron less than the target nucleus can be produced. If the proton-neutron collision is inelastic, the p,pn product can be formed as follows:

(a) All the collision products can escape without further interaction in the nucleus. The neutron must have been knocked out of a shell, which leaves the nucleus in an excited "hole" state stable to particle emission.

(b) A neutron can be left behind with an energy increase (about 8 to 16 Mev) such that the primary collision is followed by nuclear emission of only one neutron. The Coulomb barrier suppresses proton emission for all but the low-Z elements.

A p-p inelastic collision can also form the (p,pn) product by:

(c) Leaving a proton behind with an energy increase (also about 8 to 16 Mev) such that the primary collision is followed by nuclear emission of a neutron.

Elastic p-n and p-p collisions form the (p,pn) product by the same pathways as for the inelastic p-n collisions. Similar pathways also hold for the $p,2p$ reaction cross section.

An estimate of the relative contribution of processes (a) and (b) can be made by reference to the experimental cloud-chamber data on p-n and p-p collisions. Out of 134 inelastic events caused by 1.72-Bev neutrons on hydrogen gas,[15] 86 events produced neutrons by the reaction $(np \rightarrow np\pi^+\pi^-)$. The rest of the events consisted of the reactions $(np \rightarrow pp\pi^-)$ and $(np \rightarrow pp\pi^-\pi^0)$. Only two out of the 86 events, which are the only ones that can contribute to the (p,pn) cross section by process (b) produced protons with an energy as low as 40 Mev. The lowest energy neutron had a kinetic energy of 74 Mev. A study of inelastic events caused by 3.8 ± 2.4 Bev neutrons on protons showed that there were 35 $pp\pi^-$ events, 97 $pn\pi^+\pi^-$ events, 34 $pn\pi^+\pi^-\pi^0\cdots$ events (the dots refer to other possible neutral pions), and 35 events of other types that produce between two and five pions.[16] The 131 $pn\pi^+\pi^-$ and $pn\pi^+\pi^-\pi^0\cdots$ events provided only one proton with a kinetic energy less than 20 Mev.

These results can be used in the following manner. The 1.72-Bev results show that in 134 events there are no events which produce protons in the 8- to 16-Mev kinetic-energy range and are the correct type for process (b) after "inversion." Similarly, out of 201 n-p events at 3.8 Bev, one event, which would contribute to process (b) after "inversion," produced a proton in the 8- to 16-Mev kinetic-energy range. ("Inversion" of n-p collision data to p-n data should exchange neutrons for protons in the $pn\pi^+\pi^-\pi^0$ and $pn\pi^+\pi^-$ events only.) Rather than use statistical analysis for a rough determination of the relative contribution of process (b), we will determine an upper limit by assuming that if the next two events had been measured, they would contribute to process (b). Thus we have two out of 134 events and three out of 201 events which contribute to process (b). Since the rest of the events contribute to (a), the contribution of process (b) is $\leq 2\%$ of that of process (a).

The relative contribution of process (c) is more difficult to estimate, as there are no laboratory-system scatter diagrams for inelastic p-p collisions in the literature. However, with an analysis similar to that used above coupled with the p-p collision data,[23,24] we can estimate the relative contribution of process (c) to be $\leq 3\%$ of that at process (a).[25] Consequently, the relative contribution of processes (b) and (c) is $\leq 5\%$ of process (a) and can be neglected.

---

[23] M. M. Block, E. M. Harth, V. T. Cocconi, E. Hart, W. B. Fowler, R. P. Shutt, A. M. Thorndike, and W. L. Whittemore, Phys. Rev. **103**, 1484 (1955).

[24] R. M. Kalbach, J. J. Lord, and C. H. Tsao, Phys. Rev. **113**, 325, 330 (1959).

[25] Paul A. Benioff, thesis, University of California Radiation Laboratory Report UCRL-8780, July, 1959 (unpublished).

IV. THEORY

A. Development

By the use of the previously discussed approximations, the contribution to the p,pn cross section from inelastic p-n collisions [process (a)] can be found. Consider a cylindrical coordinate system whose origin coincides with the center of a nucleus and in which a proton is coming in parallel to the z axis. Then, for a given p-n inelastic interaction which produces 2 nucleons and t-2 mesons, the probability per unit path length, P_{tk}, that the incident proton gets to a point r,z,φ without interacting and collides with the kth nucleon, and all the collision products escape without further interaction is

$$P_{tk}=\exp\left[-\sigma_1\int_z^\infty \rho(R)dy\right]\times\exp\left[-\sum_{i=1}^{t}\sigma_i\int_{-\infty}^{z}\rho'(R)dy\right]\sigma_2 P_k(rz\varphi). \quad (1)$$

The first exponential factor gives the probability that the proton gets to r,z,φ without colliding with any nucleons, and the second exponential gives the probability that all the collision products escape (with 0° scattering angle) without further interaction. The increment of path length, dy, is along the path of the incident and emergent particles. Here $\sigma_2 P_k(r,z,\varphi)$ is the probability per unit path length that the incident proton collides inelastically with the kth nucleon at r,z,φ. The inelastic p-nucleon interaction cross section is σ_2, and $P_k(r,z,\varphi)$ is the normalized probability per unit volume of finding the kth nucleon at r,z,φ. The term $\rho(R)$ ($R^2=r^2+y^2$, where y is equivalent to z) gives the total nuclear density distribution in the target nucleus, $\rho'(R)$ is the same as $\rho(R)$ except that the kth nucleon has been removed from the total nucleon density distribution, because after the collision it is one of the collision products. The total interaction cross section for the incident proton with a target nucleon is σ_1. The σ_i are the nucleon-nucleon and pion-nucleon total collision cross sections, and the sum is over all t particles produced in the particular type of p-nucleon interaction under consideration. The integrals in the exponents give the total number of nucleons per unit area along the path lengths of the incident and emergent particles. The two exponential terms are the equivalent of factors used in the optical model to give the damping of the incident and emergent particle waves.[26]

If the target nucleus is in a uniform beam of bombarding protons, the cross-section contribution, σ_{tk}, to single-collision processes involving the kth nucleon is obtained by integrating P_{tk} along the path length, weighting the result by $rdrd\varphi$ and integrating over all r and φ. This gives

$$\sigma_{tk}=\int_0^{2\pi}d\varphi\int_0^\infty rdr\int_{-\infty}^{\infty}\exp\left[-\sigma_1\int_z^\infty\rho(R)dy-\sum_{i=1}^{t}\sigma_i\int_{-\infty}^{z}\rho'(R)dy\right]\sigma_2 P_k(rz\varphi)dz. \quad (2)$$

The constant σ_2 can be moved outside the integrals. If one sets σ_{tk} equal to $\sigma_2 M_{tk}$, then σ_2 can be ignored at this stage. An average of Eq. (2) over the inelastic collision types (different values of t) and energy spectrum of the scattered particles (different values of each σ_i) gives the result

$$M_k=\bar{M}_{tk}=\int_0^{2\pi}d\varphi\int_0^\infty rdr\int_{-\infty}^{\infty}\exp\left[-\sigma_1\int_z^\infty\rho(R)dy-\bar{\sigma}\int_{-\infty}^{z}\rho'(R)dy\right]P_k(rz\varphi)dz, \quad (3)$$

where $\bar{\sigma}$ is an appropriate average of $\sum\sigma_i$, and M_k may be regarded as the fractional availability of the kth nucleon in the nucleus for single-collision processes with subsequent escape of all collision products.

The factor P_k is given by

$$P_k=\int\psi_A^*\psi_A d\tau, \quad (4)$$

where ψ_A is the antisymmetric nuclear wave function. Because the integrand in Eq. (3) depends only on the space coordinates of the kth nucleon, the integration in Eq. (4) is over the spin coordinates of all the nucleons and the space coordinates of all nucleons except the kth. If the nucleus is regarded as an assembly of independent particles, ψ_A is equal to the normalized Slater determinant. Substitution of this determinant into Eq. (4) and performance of the integrations over the coordinates of all nucleons (kth excluded) gives

$$P_k=\frac{1}{A}\sum_q\int_{\text{spin space}}\psi_q^*(\tau_k)\psi_q(\tau_k)d\alpha. \quad (5)$$

The $\psi_q(\tau_k)$ represents the single-particle spin-orbit-coupled wave functions of the kth nucleon, and q stands for a set of quantum numbers needed to specify a nucleon completely. The sum is over all A sets of q, where A is the number of nucleons in the nucleus.

The factor q in Eq. (5) stands for the single-nucleon quantum numbers n,l,j,m_j,m_τ and the sum is over all occupied single nucleon states. There are $(N+P)_{nlj}$ terms in the q sum which differ only by m_j and m_τ (the isospin-projection quantum number), where $(N+P)_{nlj}$ is the number of nucleons in the nlj shell (the subscript n is the principal quantum number).

[26] S. Fernbach, R. Serber, and T. B. Taylor, Phys. Rev. **75**, 1352 (1949).

Because each nucleon in a given shell may assume any one of the m_j values, an average over the m_j values must be taken. The target nucleus is bombarded in an essentially field-free region as far as its alignment is concerned, so that each one of the m_j states is equally probable. If we separate the space and spin parts of $\psi_q(\tau_k)$ by use of Clebsch-Gordan coefficients,[27] and average over the m_j values using the operator

$$\frac{1}{2j+1}\sum_{m_j=-j}^{j},$$

we get

$$P_k=\frac{1}{A}\sum_{nlj}\sum_{m_jm_l}\frac{(N+P)_{nlj}}{2j+1}C^2(lsj;m_l,m_j-m_l)\times T_{nlj}^2(R_k)Y_{lm_l}^*(\theta_k\varphi_k)Y_{lm_l}(\theta_k\varphi_k). \quad (6)$$

The equal probability that m_j assume any value between $-j$ and j allows m_l to assume all of its values between $-l$ and l. The m_j sum can be done by use of standard procedures for manipulating Clebsch-Gordan coefficients.[27] Use of the spherical-harmonic addition theorem to remove the Y_{lm_l} factors gives[28]

$$P_k=\frac{1}{4\pi A}\sum_{nlj}(N+P)_{nlj}T_{nlj}^2(R_k). \quad (7)$$

Substituting Eq. (7) into Eq. (3) and summing over all nucleons gives for the fractional availability, M, of all the nucleons in the nucleus for single collisions ($R_k^2=r_k^2+z_k^2$)

$$M=\frac{1}{4\pi A}\sum_{k=1}^{A}\sum_{nlj}(N+P)_{nlj}\int_0^{2\pi}d\varphi\int_0^{\infty}rdr\int_{-\infty}^{\infty}\times\exp\left[-\sigma_1\int_z^{\infty}\rho(R)dy-\bar{\sigma}\int_{-\infty}^{z}\rho'(R)dy\right]T_{nlj}^2(r_k^2+z_k^2)dz. \quad (8)$$

It is shown elsewhere that Eqs. (7) and (8) hold also for j-j-coupled shell-model wave functions.[25] The k sum may be done immediately, because each term is identical, which removes the $1/A$. Likewise, the φ integration may be done, because the integrand is azimuthally symmetric.

The part of M which contributes to the p,pn reaction by processes of type (a) is obtained by limiting $(N+P)_{nlj}$ to neutrons only and limiting the sets nlj to those for which the sudden removal of a neutron with quantum numbers nlj leaves the nucleus in an excited state stable to particle emission. This gives, for $M_{p,pn}$,

$$M_{p,pn}=\sum_{\substack{\text{allowed}\\ nlj\text{ values}}}N_{nlj}M_{nlj}. \quad (9)$$

The fractional availability per neutron in the nlj shell for single-collision processes, M_{nlj}, is given by

$$M_{nlj}=\frac{1}{2}\int_0^{\infty}rdr\int_{-\infty}^{\infty}\exp\left[-\sigma_1\int_z^{\infty}\rho(R)dy-\bar{\sigma}\int_{-\infty}^{z}\rho'(R)dy\right]T_{nlj}^2(r^2+z^2)dz. \quad (10)$$

The availability, M_{nlj}, for target protons is also given by Eq. (10) if the correct value of $\bar{\sigma}$ and form of $T_{nlj}(r^2+z^2)$ are inserted.

Equation (10) holds for a variety of potential-well shapes, such as the square, harmonic-oscillator, exponential wells, etc. In this work the harmonic-oscillator well will be used for two reasons. First, it gives a finite gradient to the nuclear surface, something that has been postulated to explain the difference between the calculated and observed p,pn cross sections.[4,9,10] Second, solutions to the Schrödinger equation can be obtained in an analytic form.

An additional simplification is that for the harmonic-oscillator well, inclusion of a spin-orbit coupling term in the wave equation changes only the eigenvalues and not the wave functions. For this reason, the j subscript will be dropped from M and T in Eq. (10) ff.

The normalized radial harmonic-oscillator wave functions for the first three radial shells are[29]

$$T_{nl}=\left(\frac{\beta^{3}2^{l+2}}{\pi^{\frac{1}{2}}(2l+c)!!}\right)^{\frac{1}{2}}B_n(\beta^2(r^2+z^2))^{l/2}\times\exp\left(-\frac{\beta^2(r^2+z^2)}{2}\right), \quad (11)$$

where c and B_n are a numerical constant and simple polynomial, respectively, both depending on n. Equation (11) is normalized to give 2 upon integration over the r and z coordinates. This is necessary to remove the factor of 1/2 brought in from the removal of the spherical harmonics. The validity of this can be shown by removing the exponential factors from Eq. (10), substituting Eq. (11) into Eq. (10), and integrating over the r and z coordinates to get unity.

The density term $\rho(r^2+y^2)$ is obtained from Eq. (11) by setting $y=z$ and

$$\rho(r^2+y^2)=\frac{1}{4\pi}\sum_{nl}(N_{nl}+P_{nl})T_{nl}^2. \quad (12)$$

The sum is over all occupied n,l, shells. For a given n

[27] M. Rose, *Elementary Theory of Angular Momentum* (John Wiley & Sons, Inc., New York, 1957), Chap. III.

[28] E. Condon and G. Shortley, *The Theory of Atomic Spectra* (Cambridge University Press, London, 1957), Chaps. III and IV, pp. 53, 178.

[29] M. Mayer and J. Jensen, *Elementary Theory of Nuclear Shell Structure* (John Wiley & Sons, Inc., New York, 1955), p. 236.

and l, $N_{nl}+P_{nl}$ is the number of nucleons in the two shells obtained by setting $j=l+\frac{1}{2}$ and $j=l-\frac{1}{2}$. The $1/(4\pi)$ is the normalizing factor. Equation (12) neglects any effect of the Coulomb force on the total nuclear density distribution. The error due to this neglect should not be large unless the radial proton distribution is markedly different from that given by Eq. (12). The factor $\rho'(r^2+y^2)$ is obtained from Eq. (12) by subtracting one from that value of N_{nl} whose subscripts are the same as those on M_{nl}.

For several reasons Eq. (12) was used for the nuclear-density distribution, rather than the simpler equation

$$\rho(R)=\rho^0\{\exp[(R-d)/\alpha]+1\}^{-1}$$

obtained for most target nuclei from the electron-scattering results.[30] One reason is that a single model is used by which the complex dependence of Eqs. (10), (11), and (12) on β can be removed. Another is that there is only one adjustable parameter, β, rather than three—β, d, and α. The use of Eq. (12) also ensures a consistent nucleus whose total density distribution is built up out of the distributions of the individual nucleons.

The substitutions $u=\beta r$, $v=\beta z$, $w=\beta y$, simplify the complex β dependence remarkably. Making these substitutions and putting Eqs. (12) and (11) into Eq. (10) gives

$$M_{nl}=\frac{2^{l+1}}{\pi^{\frac{1}{2}}(2l+c)!!}\int_0^\infty udu\int_{-\infty}^{\infty}\Big\{B_n{}^2(u^2+v^2)^l \times\exp\Big[-u^2-v^2-\frac{\sigma_1\beta^2}{\pi^{\frac{3}{2}}}\int_v^\infty\rho(u^2+w^2)dw -\frac{\bar{\sigma}\beta^2}{\pi^{\frac{3}{2}}}\int_{-\infty}^{v}\rho'(u^2+w^2)dw\Big]\Big\}dv, \quad (13)$$

where

$$\rho(u^2+w^2)=\sum_{nl}(N_{nl}+P_{nl})\frac{2^lB_n{}^2}{(2l+c)!!}(u^2+w^2)^l \times\exp(-u^2-w^2), \quad (14)$$

and $\rho'(u^2+w^2)$ bears the previously mentioned relationship to $\rho(u^2+w^2)$. Values of $B_n{}^2$ and c for the different values of n are given below:

n	c	$B_n{}^2$
1	1	1
2	3	$2\{l+\frac{3}{2}-[u^2+(v^2 \text{ or } w^2)]\}^2$
3	5	$2\{(l+\frac{5}{2})(l+\frac{3}{2})-(2l+5)[u^2+(v^2 \text{ or } w^2)]+[u^2+(v^2 \text{ or } w^2)]^2\}^2$.

The double factorial stands for the product of all the odd integers less than or equal to $2l+c$.

[30] Robert Hofstadter, *Annual Review of Nuclear Science* (Annual Reviews, Inc., Palo Alto, California, 1957), Vol. 7, p. 231.

For ease in interpreting the results, the harmonic-oscillator spring constant β in the exponents of Eq. (13) can be written as

$$\beta^2=g/A^{\frac{1}{3}}, \quad (15)$$

where g is given by

$$g=0.847/r_0{}^2, \quad (16)$$

and r_0 is the half central-density radius constant. Equations (15) and (16) are derived in Appendix II. As is discussed there, Eq. (16) is only approximately correct and gives values of r_0 which are in error by from $+3\%$ for F^{19} to -9% for Ce^{142} when compared to values of r_0 obtained in an exact manner.

B. Integral Evaluation

Equation (13) cannot be integrated analytically, so it was integrated by the use of Simpson's rule and the IBM-701 electronic computer. The interval size used and the upper limits of integration were chosen such that the error made in the numerical integration of M_{nl} was less than or equal to 1%.

The computer was also programmed to print out the values of the integrand of the u,v integration given in Eq. (13) and the corresponding values of u and v. This was done in order to find out by means of contour plots what part of the nucleus contributed most to M_{nl}.

The value of the total p-nucleon collision cross section, σ_1, was set equal to 30 mb.[22] The total exit collision cross section, $\bar{\sigma}$, was estimated from the 3.8-Bev cloud chamber data to be 180 mb. The derivation of the value of $\bar{\sigma}$ and corrections due to refinements in the values of σ_1, and $\bar{\sigma}$ are discussed later. Reasonable values of $g=0.50$ and 1.00 were chosen for most calculations.

The target isotopes chosen for the calculation of values of M_{nl} were C^{12}, N^{14}, O^{16}, F^{19}, Na^{23}, A^{40}, Ni^{58}, Cu^{65}, As^{75}, Nb^{93}, Cd^{111}, In^{115}, I^{127}, Ce^{142}, Os^{192}, and U^{238}. The neutron- and proton-shell occupation numbers for all these target isotopes except U^{238} were taken from Mayer and Jensen.[31] The U^{238} occupation numbers were obtained from a Nilsson diagram for a deformed nucleus.[32] From the above data, values of M_{nl} for several shells for several values of g for different isotopes were determined, and contour plots obtained for some cases. For a few shells, values of M_{nl} for different values of $\bar{\sigma}$ or σ_1 with g constant were obtained.

C. Contour Plots

Figures 1 and 2 are contour plots of the integrand of Eq. (13) for two cases—the Cu^{65} $1f$ shell and the Ce^{142}

[31] Reference 29, pp. 74–81.

[32] The author thanks Dr. Frank Stephens for supplying the occupation numbers of the upper shells of U^{238}.

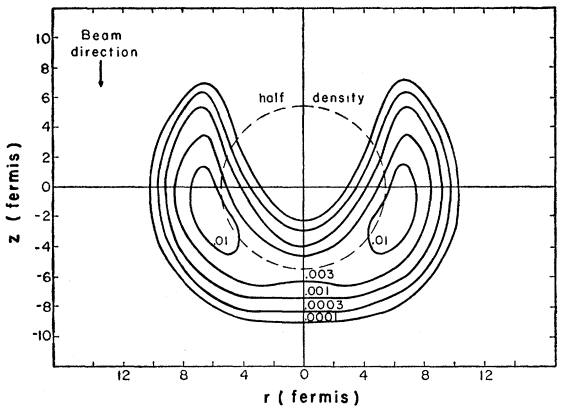

FIG. 1. Contour plot of the $1f$ shell of Cu^{65}; $\sigma_1=30$ mb, $\bar{\sigma}=180$ mb, $g=0.50$. The broken line circle gives the half-central-density radius.

$2f$ shell—i.e., of

$$Q_{nl}=\frac{2^l}{(2l+c)!!}B_n^2(u^2+v^2)^l \times\exp\left[-u^2-v^2-\frac{\sigma_1 g}{A^{\frac{1}{3}}\pi^{\frac{3}{2}}}\int_v^\infty \rho(u^2+w^2)dw - \frac{\bar{\sigma}g}{A^{\frac{1}{3}}\pi^{\frac{3}{2}}}\int_{-\infty}^v \rho'(u^2+w^2)dw\right], \quad (17)$$

for various values of $r=u/\beta$ and $z=v/\beta$. The contour lines connect points r,z which give equal values of Q_{nl}. The dashed circle is the locus of points for which the value of the total nuclear density, $\rho(u^2+v^2)$ from Eq. (14), is one half that at the center of the nucleus. The three-dimensional "picture" is obtained by rotating the contour maps about the z axis.

It is immediately apparent from Figs. 1 and 2 that the main contribution to M_{nl} is strongly weighted towards the surface region of the nucleus. In fact for the $2f$ Ce^{142} shell the main contribution is quite far out from the half-density circle. Because the p,pn reaction is limited to the topmost few shells, these contour plots clearly indicate that the p,pn reaction is mainly a surface reaction. This is why the errors introduced by "lifting" the free n-p scattering data into the nucleus should be small. The secondary peak in Fig. 2 for the Ce^{142} $2f$ shell is not visible, as it is too far inside the nucleus and is suppressed by the exponent integrals in Eq. (17). The contours also show that most of the contribution to M_{nl} comes from the downbeam side of the nucleus. This asymmetric distribution about the $z=0$ plane comes from the fact that $\bar{\sigma}$ is much bigger than σ_1; the distribution becomes symmetric about the $z=0$ plane as $\bar{\sigma}$ approaches σ_1.

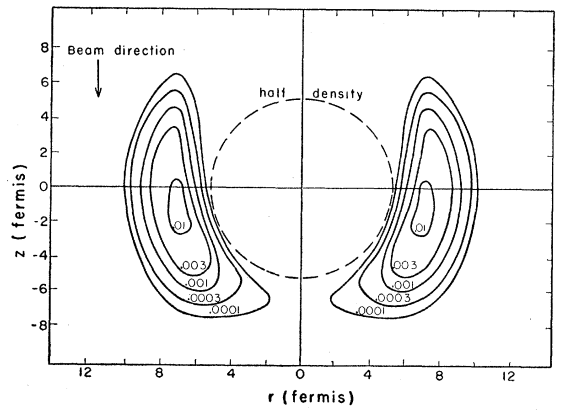

FIG. 2. Contour plot of the $2f$ shell of Ce^{142}; $\sigma_1=30$ mb, $\bar{\sigma}=180$ mb, $g=1.00$.

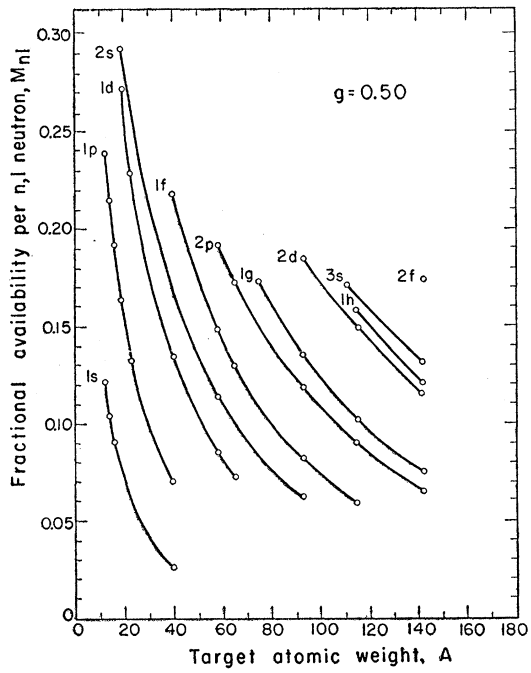

FIG. 3. The dependence of M_{nl} on A, the target atomic weight, for different shells; $\sigma_1=30$ mb, $\bar{\sigma}=180$ mb, and $g=0.50$.

D. M_{nl} Results

Figures 3 and 4 show the dependence of M_{nl} on the atomic weight A, of the target nucleus for two values of g, 0.50 and 1.00. These curves may be used for interpolating to target isotopes other than those for which M_{nl} values were computed. The difference between the values of M_{nl} due to different neutron and proton occupation numbers for isobaric target elements for any given shell would be expected to be small. This was shown by computing values of M_{1f} and M_{1h} for Ga^{65} and Nd^{142} ($\sigma_1=30$ mb, $\bar{\sigma}=180$ mb, $g=1.00$). The value of M_{1f} for Ga^{65} (two less $1f_{5/2}$ neutrons and two more $2p_{3/2}$ protons than Cu^{65}) was found to be less than M_{1f} for Cu^{65} by 0.3%. For Nd^{142} (no $2f_{7/2}$

neutrons and two $2d_{5/2}$ protons), the value of M_{1h} was higher than for Ce^{142} by 1.2%. The effect of changing the configuration of the top three nucleons of F^{19} from $(1d_{5/2})^2$ $(2s_{1/2})^1$ to $(2s_{1/2})^3$ was found by computing M_{2s} for both forms.[33,34] The value of M_{2s} for the $(1d_{5/2})^2$ $(2s_{1/2})^1$ configuration was lower than that for $(2s_{1/2})^3$ by 1.4% ($\sigma_1=30$ mb, $\bar{\sigma}=180$ mb, $g=0.50$).

The shell structure in Figs. 3 and 4 is quite evident in that for a given A there appears to be a close correlation between the values of M_{nl} and the total energy of the n,l shell in the potential well. The correlation is due to the fact that for a potential well with sloping sides, the mean square radius of a shell is larger the higher the shell is in the potential well. Here M_{nl} would be expected to be larger for bigger values of the mean square radius, because the exponent integrals in Eq. (13) are smaller. In Figs. 3 and 4 the

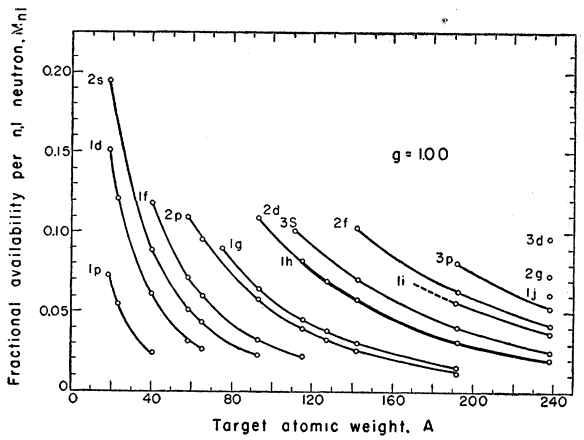

FIG. 4. The dependence of M_{nl} on A, the target atomic weight for different shells; $\sigma_1=30$ mb, $\bar{\sigma}=180$ mb, and $g=1.00$.

curves of M_{nl} as a function of target atomic weight were not extended beyond the point at which the shells are so far down in the well that their availability to the p,pn cross sections is highly improbable. This is the reason why all the curves appear to have a cutoff at the low M_{nl} end.

A comparison of the M_{nl} values for the same target shells for the two values of g, the spring-constant parameter, shows that the g dependence of M_{nl} can be approximated by

$$gM_{nl}=\text{constant}. \tag{18a}$$

This equation was checked over an extended g range for several F^{19}, Cu^{65}, and Ce^{142} shells. Figure 5 gives the Ce^{142} results. The curves for F^{19} and Cu^{65}, which are similar to those for Ce^{142}, are given elsewhere.[25] The curves in Fig. 5 show that Eq. (18a) is a good approximation if the amount of g extrapolation is not too great. Equation (18a) is very useful for interpolating

[33] S. Unna and I. Talmi, Phys. Rev. **112**, 452 (1958).
[34] G. Rakavy, Nuclear Phys. **4**, 375 (1957).

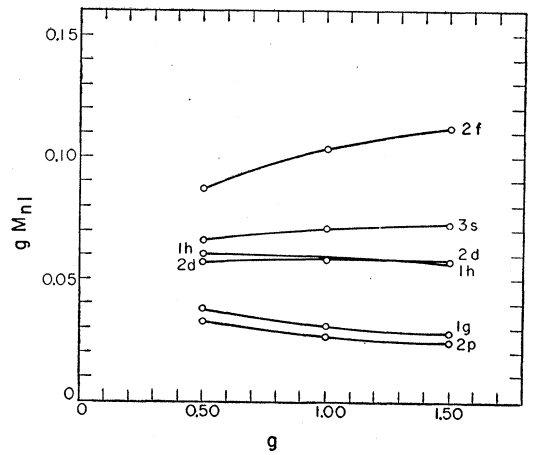

FIG. 5. Plot of gM_{nl} as a function of g, the nuclear density distribution parameter, for Ce^{142} shells; $\sigma_1=30$ mb, $\bar{\sigma}=180$ mb.

the M_{nl} results given in Figs. 3 and 4 to other g values. If desired, Fig. 5 (or Figs. 3 and 4 for $A<142$) can be used to roughly correct Eq. (18a).

Figure 6 gives curves of M_{nl} versus $\bar{\sigma}$, the average total exit cross section, for the F^{19} $1d$ shell, the Cu^{65} $1f$ shell, and the Ce^{142} $1h$ shell. It is seen that this dependence can be represented by

$$(\bar{\sigma})^{\frac{1}{2}}M_{nl}=\text{constant}. \tag{18b}$$

Similarly, for these three shells as well as a few others, M_{nl} was determined for several values of σ_1, the total p-n collision cross section. The results show that, similarly, we have

$$(\sigma_1)^{\frac{1}{2}}M_{nl}=\text{constant}. \tag{18c}$$

It would be expected, from an examination of Eqs. (13) and (15) that the g dependence would be greater than the σ_1 or $\bar{\sigma}$ dependence because g occurs as a factor of both exponent integrals, whereas σ_1 and $\bar{\sigma}$ each occur as a factor of only one of the integrals.

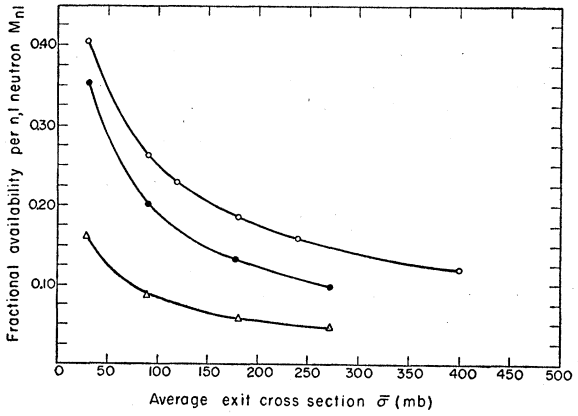

FIG. 6. Plot of M_{nl} as a function of $\bar{\sigma}$ the average total exit cross section. ○ refers to the F^{19} $1d$ shell, $\sigma_1=30$ mb, $g=0.80$; ● refers to the Cu^{65} $1f$ shell, $\sigma_1=30$ mb, $g=0.50$; △ refers to the Ce^{142} $1h$ shell, $\sigma_1=30$ mb, $g=1.00$.

Also the points of maximum contribution to M_{nl} obtained from the contour plots are points at which the two exponent integrals, each with their associated factors, would appear to be similar in value.

E. Elastic (p,pn) Collision Contribution

The total (p,pn) reaction cross section is obtained by adding to Eq. (9) a term giving the contribution from the elastic p-n collisions. The total cross section is equal to

$$\sigma_{p,pn}=\sum_{\substack{\text{allowed}\\ \text{shells}}}(M_{nl}\sigma_{\text{inel}}+S_{nl}\sigma_{\text{el}})N_{nlj}, \qquad (19)$$

where the second term on the right gives the contribution from the elastic fraction of the p-n collision. A computation of S_{nl} by the same methods as used for M_{nl} represents a formidable undertaking. One difficulty is that the zero scattering angle approximation is invalid. A much better approximation for the elastic collisions is to take the scattering angle to be 90° lab. Also the Pauli principle would have to be taken into account specifically as the scattered nucleon has a high probability of gaining a relatively small amount of energy. For 5.7-Bev protons on free neutrons one-half the elastically scattered neutrons have kinetic energies of $\leq$60 Mev and lab scattering angles between 78° and 90°. To evaluate an expression like Eq. (13) but containing the exclusion principle and the 90° scattering angle approximation would be prohibitively long in terms of machine time as there would be five successive integrations and a more complex integrand. Consequently the following approximate method to determine S_{nl} will be used.

One can approximate S_{nl} by writing

$$S_{nl}\simeq FM_{nl}',$$

where F, the amount by which M_{nl}' should be reduced to account for the escape of the struck neutron, is independent of the shell quantum numbers and target atomic weight. The term M_{nl}' is given by Eq. (13) with $\bar{\sigma}$ set equal to σ_1 and accounts for the entrance, elastic collision, and exit of the incident proton which suffers negligible energy loss and angular deviation. Use of Eq. (18b) gives the result

$$M_{nl}'=(\bar{\sigma}/\sigma_1)^{\frac{1}{3}}M_{nl}. \qquad (20)$$

It can be seen from Fig. 6 that for $\bar{\sigma}$=30 mb this equation is correct to within 10% when summation over the allowed shells in Eq. (19) is allowed for. Combining the above three equations and recalling that $\sigma_1=\sigma_{\text{inel}}+\sigma_{\text{el}}$ gives

$$\sigma_{p,pn}=\sigma_1\left[1+f\left(F\left(\frac{\sigma}{\sigma_1}\right)^{\frac{1}{3}}-1\right)\right]\sum_{\substack{\text{allowed}\\ \text{shells}}}N_{nlj}M_{nl}, \qquad (21)$$

where f is the fraction of the total (p,n) cross section which is elastic. It should be recalled that the j subscript is lacking on M_{nl} because of the j degeneracy in the harmonic oscillator model.

V. APPLICATION TO NUCLEI

Before Eq. (21) can be applied to experimental (p,pn) cross sections, the factors appearing before the summation sign have to be evaluated; in particular both $\bar{\sigma}$ and F must be determined. The 3.8-Bev n-p cloud chamber data will be used to obtain a value of $\bar{\sigma}$. The value of $\bar{\sigma}$ for 1.72-Bev n-p collisions will just be presented when needed even though it was obtained in the same manner. It should be recalled that M_{nl} also depends on σ_1 and $\bar{\sigma}$.

A. Determination of $\bar{\sigma}$

The average total exit cross section, $\bar{\sigma}$, was determined by first finding the distribution of the values of $\sum\sigma_i$ from the experimental laboratory scatter diagrams of the high-energy n-p inelastic collisions in the following manner: The analysis of inelastic events caused by 3.8±2.4-Bev neutrons on protons[16] shows that 83% of the events consist of the reactions $pn\rightarrow pp\pi^-$ (18%), $pn\rightarrow pn\pi^+\pi^-$ (48%), and $pn\rightarrow pn\pi^+\pi^-\pi^0\cdots$ (17%). The rest of the events (17%) consist of small amounts of several types of two-, three-, and four-meson producing events. Because there are so many different types of these events, the 17% will be neglected and the inelastic events will be assumed to consist only of the three main types given above (with their percentage occurrence increased by 100/83). The analysis further shows that in the c.m. system the intensity distribution of the emitted protons from the $pp\pi^-$ reaction is strongly peaked forward and backward, and that of the pions is peaked forward. The neutron and negative-pion intensity is peaked forward for the $pn\pi^+\pi^-$ reaction, while the intensity for the protons and positive pions is peaked in the backward direction. For the $pn\pi^+\pi^-\pi^0$ reactions, the proton distribution is peaked in the forward direction, and the charged pion distributions are isotropic.

These c.m. intensity distributions have to be "inverted" because they are for n-p collisions, not p-n collisions. This inversion merely exchanges forward c.m. intensity peaks for backward c.m. peaks and vice versa. In the succeeding discussion this "inversion" is included. The momentum distribution in the laboratory system for each of the various particles emitted for each type of inelastic event[16] was divided into several sections, and the number and midpoint kinetic energy of the particles in each section was tabulated. From the published pion-nucleon and nucleon-nucleon excitation functions,[9,35,36] a cross section, σ_i, was

[35] S. Lindenbaum, *Annual Review of Nuclear Science* (Annual Reviews, Inc., Palo Alto, California, 1957 Vol. 7, p. 317.
[36] Wilmot Hess, Revs. Modern Phys. **30**, 368 (1958).

associated with the midpoint energy for the given type of particle passing through nuclear matter that was assumed to be half neutrons and half protons. From the fact that forward and backward c.m. distributions correspond to low (inverted) and high (inverted) kinetic-energy laboratory distributions, respectively, "events" were reconstructed. For the $(p,p\pi^-)$ reaction, a proton and π^- out of the lowest energy range were combined with a proton in the highest energy range, the three values of σ_i were found, and the three particles were removed from the distribution. This process was repeated until all the particles were used up. Similarly for the $pn\pi^+\pi^-$ events, a neutron and π^- each from their respective lowest kinetic-energy section were combined with a proton and π^+ each from their respective highest kinetic-energy section, and the four values of σ_i were found, etc. Scatter diagrams were not available for the neutrons and π^0's from the $pn\pi^+\pi^-\pi^0$ reaction. Somewhat arbitrarily the π^+'s and π^0's were considered to have the same backward peaking in the c.m. system, and the neutron and π^- distributions were taken to be peaked in the forward c.m. direction. The π^0 and neutron momentum distributions were taken to be the same as those for positive pions and protons, respectively. A proton and π^+ and π^0 from their respective lowest kinetic-energy sections were then combined with a π^- and neutron in their respective highest kinetic-energy sections, and the five values of σ_i were found, etc. Finally the appropriate values of σ_i were then combined to give values of $\sum_{i=1}^{t}\sigma_i$, where t equals 3, 4, and 5 for the $pp\pi^-$, $pn\pi^+\pi^-$, and $pn\pi^+\pi^-\pi^0$ events, respectively.

These $\sum\sigma_i$ must still be weighted by the associated values of M_{nl}. This was done by computing values of M_{nl} for three representative shells (the shells are given in Table I) for possible values of $\bar{\sigma}$ ranging from 30 mb to 275 to 400 mb. Plots of M_{nl} versus $\bar{\sigma}$ were used to weight the $\sum\sigma_i$ distribution accordingly. Finally the M_{nl} weighted distribution was averaged over inelastic-event types to give a value of $\bar{\sigma}$ equal to 180 mb. It was found that this value of $\bar{\sigma}$ was quite insensitive to changes in shell quantum numbers or target atomic weights.

This value of $\bar{\sigma}$ must still be corrected for exclusion-principle effects on the σ_i and meson absorption in the nucleus. The correction on σ_i due to the exclusion principle can be roughly estimated by determining the maximum target-nucleon kinetic energy, T_m, at the point $R_m=(u^2+v^2)^{\frac{1}{2}}/\beta$ at which the contour plot of M_{nl} shows a maximum. For this purpose, we can assume the nucleus to be a degenerate Fermi gas of depth T_m. Use of the kinetic energy and particle type associated with each cross section, σ_i, and T_m in the published equations[37–39] gives the cross-section reduction factor. We can determine T_m from Eq. (B2) of Appendix II; T_0 is the central kinetic energy of the highest occupied shell.[40,41] The substitution of Eqs. (15) and (B6) of Appendix II into Eq. (B2) and replacement of r by R_m gives T_m as a function of g. Table I gives T_m for two values of g for three representative shells. The value of T_m was taken to be 12 Mev. With this value, the σ_i were now corrected for the exclusion-principle effect. For σ_i associated with mesons, the meson absorption cross section was included.[9] The correct σ_i values were then combined and weighted by the method just discussed to give a final average value of $\bar{\sigma}$ equal to 168 mb. This final $\bar{\sigma}$ was found to be quite insensitive to changes in g and to be the same for each of the three shells for which it was derived.

TABLE I. The Fermi energy, T_m, at the M_{nl} contour plot maximum.

	$1d$ shell of F^{19}		$1f$ shell of Cu^{65}		$1h$ shell of Ce^{142}	
g	0.5	0.8	0.5	0.8	1.0	1.5
T_m(Mev)	13	15	10	11	12	16

B. Determination of F

The slow neutron escape factor, F, can be estimated by dividing the spectrum of the energy gain of the struck neutron into three parts. If the struck nucleon gains less than 8 Mev, it cannot escape from the nucleus, so that the collision does not contribute to the p,pn reaction. If the struck neutron gains between 8 and 18 Mev, the collision will always contribute to the p,pn reaction because if it does not escape, [process (b)], the resultant excited nucleus will usually evaporate only one neutron. Finally, if the target neutron gains 18 Mev or more it must escape. This division into three parts with boundaries of 8 and 18 Mev is not meant to be accurate. It does, however, allow F to be easily estimated.

The fraction of elastic 5.7-Bev p-n collisions that gives the struck neutron a gain of $\geqslant 18$ Mev [similar to process (a) for inelastic p-n collisions] is calculated from Eq. (A4) $(n=36)$[21,22] to be 0.79. For this fraction, a reduction of M_{nl}' by roughly one half will be assumed. This is arrived at by assuming that, similar to the inelastic collisions, most of the contribution to S_{nl} comes from collisions in the nuclear-surface region. For an elastic surface collision, the struck nucleon has roughly a probability of one half to be going away from or towards a lot of nuclear matter. If it is moving towards most of the nucleus it will probably interact, because the interaction mean free path is small for nucleons with more than 20 Mev kinetic energy.[42] If it is moving away from most of the nucleus, it is likely

[37] E. Clementel and C. Villi, Nuovo cimento **2**, 176 (1955).
[38] I. Ivanter and L. Okum, J. Exptl. Theoret. Phys. (U.S.S.R.) **32**, 402 (1957) [translation: Soviet.-JETP **5**, 340 (1957)].
[39] R. Sternheimer, Phys. Rev. **106**, 1027 (1957).
[40] W. Frahn and R. Lemmer, Nuovo cimento **6**, 1221 (1957).
[41] Reference 29, pp. 40, 41.
[42] L. Elton and C. Gomes, Phys. Rev. **105**, 1027 (1957).

to escape without interaction. Various other effects such as the exclusion principle, reflection at the nuclear surface, production of the $\geqslant$18-Mev energy-gain neutron further inside the nucleus, etc., are ignored for this rough determination. Consequently, the contribution to F from this part of the elastic p-n collisions is $\frac{1}{2}(0.79)=0.4$.

Elastic 5.7-Bev p-n collisions that give the struck neutron an energy gain between 8 and 18 Mev have a probability of occurrence of 0.1 [Eq. (A4), Appendix I]. Since all of these collisions contribute to the p,pn case, as far as the struck neutron is concerned, the contribution to F is 0.1. There is a smaller contribution from a process similar to process (c) for the inelastic p-p case where a p-p collision occurs leaving a proton with a kinetic energy gain between 8 and 18 Mev. This contribution will be neglected, as the 0.1 given above which also holds for p-p collisions must be multiplied by factors that take account of the fact that the slower proton must not leave and the p-p collisions with resulting low nuclear excitation are less likely than are p-n collisions for all but the low-Z elements. Consequently, F is set equal to the sum of the first two contributions, which is 0.5.

It is easy to set upper and lower limits on F if one neglects the contribution mentioned above from p-p elastic collisions. If one assumes that the nucleus is completely transparent to the struck neutron, then for $E_p=5.7$ Bev, $F=0.9$. The fact that collisions in which the neutron energy gain is <8 Mev can never contribute to the p,pn reaction sets this upper limit for F. Similarly the lowest F can be is 0.1 since the region of energy gain between 8 and 18 Mev is always available to the p,pn reaction. This limit corresponds to a nucleus which is completely black to the struck neutron. Thus one has $0.1<F<0.9$ and the chance of $F=0.5$ corresponds to the nucleus being "half black" to the struck neutron when its energy gain is $\geqslant$18 Mev.

This method of determining $F=0.5$ is very rough and would appear to render meaningless any information obtained from an application of the results given in the previous sections. However, it will be shown in the next section that large errors in F contribute only small errors to the final results.

C. (p,pn) Reaction Cross-Section Equations

The fraction of 5.7-Bev p-n collisions that are elastic is not known, so f will be taken from the 6.2-Bev p-p scattering data as equal to 0.24 ± 0.06.[21] The factor, σ_1, will be set equal to the recent experimental value of 33.6 ± 1.6 mb for 4.5 Bev neutrons on protons.[43] The value of M_{nl} can be corrected for this new value of σ_1 by the use of Eq. (18c). The previously mentioned correction stemming from the fact that $\bar{\sigma}$ should be 168 mb instead of 180 mb can now be included by use of Eq. (18b). The values of M_{nl} obtained from Figs. 3 and 4, when multiplied by $(30/33.6)^{\frac{1}{2}}(180/168)^{\frac{1}{4}}$, can consequently be used in Eq. (21). Substitution of the values given above for f and F ($\bar{\sigma}=168$ mb and $\sigma_1=33.6$ mb) gives the result (in mb)

$$\sigma_{p,pn}=(34\pm2)\sum_{\substack{\text{allowed}\\\text{shells}}}N_{nlj}M_{nl}. \tag{22}$$

Use of other 6.2-Bev p-p scattering data to determine f and σ_1 gives the same numerical constant in Eq. (22).[24]

Similarly for a bombarding energy of 3 Bev, the factors appearing in Eq. (21) can be evaluated. A determination of $\bar{\sigma}$ from the 1.72-Bev neutron-hydrogen collision work[15] in the same manner as for the 3.8-Bev neutron data including the exclusion principle for $T_m=12$ Mev gives $\bar{\sigma}=160$ mb. The values of σ_1 will be taken to be 38 ± 2 mb. This value is a linear interpolation between the 1.4 Bev[36] and 4.5 Bev[43] n-p cross sections for a bombarding energy of 3.0 Bev. The fraction, f, of σ_1 which is elastic is taken from the 2.75-Bev p-p collision data to be 0.37 ± 0.04.[23] As before, F is approximately 0.5. Substituting these values into Eq. (21) and correcting for the fact that M_{nl} is calculated for $\bar{\sigma}=180$ mb and $\sigma_1=30$ mb gives for 3-Bev protons incident on nuclei

$$\sigma_{p,pn}=(36\pm2)\sum_{\substack{\text{allowed}\\\text{shells}}}N_{nlj}M_{nl}. \tag{23}$$

The error limits with the numerical constants in Eqs. (22) and (23) are not meant to be absolute. They include the error limits of σ_1, f, and the 1% on M_{nl} and do not include any contribution for F.

It can be seen now that the error contributed by the rough method of determining F is small. It seems reasonable to require that $0.25\leq F\leq0.75$, i.e., the nucleus can't be either completely black or completely transparent to the struck target neutron. With these limits for F the corresponding limits for the numerical constant in Eq. (22) become 29 and 38 mb, respectively. Thus it is reasonable to expect that the value of the numerical constant is in error by less than 15%. This large reduction of the uncertainty in F comes from the factor, f, in Eq. (21). This is one of the main reasons for restricting this treatment to the multi Bev bombarding energy region where f is small.

It turns out that this error limit of 15% is smaller in most cases than the error in the experimental value of $\sigma_{p,pn}$. Furthermore the actual comparison of experimental p,pn cross section data through Eqs. (22) and (23) will be made through the radius parameter, r_0, given in Eq. (16). Since r_0 enters in Eqs. (22) and (23) through Eq. (18a) as r_0^2, the percentage error in r_0 stemming from the uncertainty in F will be further reduced to 7%. The error in r_0 for 3-Bev data will be slightly larger than 7% as f is larger. An error limit of 7% is satisfactorily small in view of the errors in the

[43] V. Perez-Mendez, J. H. Atkinson, W. N. Hess, and R. W. Wallace, Bull. Am. Phys. Soc. 4, 253 (1959).

experimental values of $\sigma_{p,pn}$ and the approximations made is this work.

D. Energy Independence of $\sigma_{p,pn}$ in the Bev Region

Equations (22) and (23) show that the theory developed here satisfies the requirement that the (p,pn) cross sections be independent of the bombarding energy in the Bev region. The decrease with increasing energy shown in these equations is less than 10% and is within the experimental-error limits on the experimental (p,pn) cross sections. At first sight it seems surprising that the cross sections do not decrease with increasing energy, because the meson multiplicity, which affects $\bar{\sigma}$, is dependent on the bombarding energy. However, this dependence is not strong, as can be seen from the mean meson multiplicities of 1.8 and 2.2 for neutrons of 1.7-Bev and 3.8-Bev average energy, respectively.[15,16] The effect of the extra 0.4 meson at 3.8 Bev is reduced by the fact that, as has been discussed, all the $\sum\sigma_i$ terms, which make up $\bar{\sigma}$, are weighted by M_{nl}. This weighting tends to suppress reactions with high meson multiplicity whose abundance is quite sensitive to the bombarding energy.

The (p,pn) cross section is also dependent on $\sigma_1^{\frac{1}{3}}$ as can be seen from Eqs. (18) and (21). The square-root dependence and the relative constancy of σ_1 in the Bev region help to give the independence of $\sigma_{p,pn}$ from the bombarding energy.

E. Inherent Uncertainties Due to Nuclear Model Chosen

Before the theoretical results are compared with experimental data it is worthwhile to stress the fact that the nuclear model used in the foregoing calculations does not represent real nuclei. One fault of the model used in the calculations is that the harmonic-oscillator well was used instead of the more realistic inverse exponential well. It is difficult to estimate how much the values of M_{nl} would be changed if the inverse exponential well were used. Both the density-distribution terms and the radial wave functions in Eq. (11) ff would be affected. Furthermore, the degeneracy in the two values of M_{nl} for different j but same nl values would be removed.

Another fault is that some effects of nucleon-nucleon interactions, e.g., j-j coupling, have been neglected. Even though Eqs. (7) and (8) hold for j-j coupling, the radial wave functions and the density terms would be altered in a complex manner. This would induce further changes in M_{nl}. In addition to this effect, Eqs. (9), (19), and (21 to 23) would have to be altered under any nucleon-nucleon coupling scheme. This change arises because the sudden removal of a nucleon from a shell will leave the product nucleus in any one of several possible parent states. Any one of these parent states, when coupled to the nlj nucleon, gives the ground state of the target nucleus. Since some of these parent states may be unstable to particle emission, a factor ≤ 1 should be included inside the nlj sum of Eq. (9) and the sum should be extended over all nlj shells of the nucleus. This factor is the sum of the squares of the appropriate fractional-percentage coefficients of all the parent states stable to particle emission. This factor tends to unity or zero as the nucleon-nucleon interaction becomes weaker and, in the limit of the independent-particle model, becomes equal to either 0 or 1, giving Eq. (9) ff. For closed-shell target nuclei, Eqs. (9), (19), and (21 to 23) are valid as written, because there is only one possible parent state even with nucleon-nucleon coupling.

The difficulties mentioned above which are caused by differences between real nuclei and the model chosen here add an element of uncertainty to any comparison of theory with experiment. In spite of this, we shall proceed to see what can be learned from a simple independent-particle model while keeping the above discussion in mind.

VI. RESULTS

Two variables are now left in Eqs. (22) and (23)—which shells are available and the value of g [or r_0 by Eq. (16)], the nuclear-density-distribution parameter. A correct calculation of which shells are available, i.e., which neutron-hole states of the product nucleus have small particle-emission widths compared to the gamma-emission widths, is quite beyond the scope of this work. However, one can use the eigenvalues of a reasonable independent particle model as a guide to determine which shells are available and then use the p,pn cross sections with Eqs. (18a) and (22) or (23) and Figs. 3 or 4 to determine g or r_0. These values of r_0 can be compared with values obtained by other experimental methods. Later another method of treating the data which considers both the shell availability and r_0 as unknowns will be discussed.

A. Radius-Parameter Determinations

The independent particle calculations of Ross, Mark, and Lawson,[12] which appear to be successful in predicting the experimentally observed shell filling, will be used here as a guide to determine the excitation energy of neutron-hole states in various shells. The availability of a shell is determined by subtraction of the excitation energy of the neutron-shell hole state from the highest particle-stable excitation energy of the product. Only if the result is greater than zero is the shell available.

The highest particle-stable excitation energy of the product nucleus is that excitation energy for which the total particle-emission width is roughly equal to the gamma-emission width. If a neutron is the least-bound particle, its binding energy is usually the highest particle-stable excitation energy. If a proton is the

TABLE II. (p,pn) cross sections and nuclear-density-distribution parameters.[a]

(p,pn) product	Proton bombarding energy (Bev)	(p,pn) cross section (mb)	Reference	Target nucleus available shells				g	r_0
C^{11}	3.0	29.8±1.6 26.7±1	44 45	$1p_{3/2}$ (4)				0.58±0.04 0.65±0.04	1.21±0.04 1.14±0.04
	5.7	29.8±1.6	44	$1p_{3/2}$ (4)				0.55±0.04	1.24±0.04
N^{13}	3.0	4.0±2.4	4	$1p_{1/2}$				0.98±0.58	1.10±0.36
	5.7	7.3±0.7	1	(1)				0.50±0.06	1.31±0.08
O^{15}	5.7	33±5	1	$1p_{1/2}$ (2)	$1p_{3/2}$ (4)			0.60±0.10	1.21±0.10
F^{18}	3.0	28±4	4	$1d_{5/2}$				0.35±0.06	1.57±0.14
	5.7	19±2	1	(2)				0.49±0.06	1.32±0.08
Na^{22}	5.7	31±5	1	$1d_{5/2}$ (4)				0.50±0.09	1.32±0.12
Fe^{53}	3.0	45±7	4	$1f_{7/2}$ (8)	$1d_{3/2}$ (4)	$2s_{1/2}$ (2)		0.72±0.13	1.10±0.10
Mn^{54}	6.2	44±10	46	$2p_{3/2}$ (2)	$1f_{7/2}$ (8)	$1d_{3/2}$ (4)		0.75±0.20	1.07±0.14
Ni^{57}	3.0	37±6	4	$2p_{3/2}$ (2)	$1f_{7/2}$ (8)	$1d_{3/2}$ (4)		0.89±0.15	0.99±0.09
Cu^{62}	3.0	66±14	4	$1f_{5/2}$	$2p_{3/2}$	$1f_{7/2}$		0.56±0.12	1.25±0.14
	5.7	46±7	2	(2)	(4)	(8)		0.76±0.13	1.07±0.10
Cu^{64}	3.0	66±7	4	$1f_{5/2}$	$2p_{3/2}$	$1f_{7/2}$		0.62±0.07	1.17±0.07
	5.7	71±6	2	(4)	(4)	(8)		0.54±0.06	1.26±0.07
Zn^{63}	3.0	68±11	4	$1f_{5/2}$ (2)	$2p_{3/2}$ (4)	$1f_{7/2}$ (8)		0.54±0.10	1.27±0.12
Mo^{99} Nb^{99b}	3.0	72±12[c]	4	$1g_{7/2}$ (2) $1g_{9/2}$ (2)	$2d_{5/2}$ (6) $2p_{1/2}$ (2)	$1g_{9/2}$ (10) $1f_{5/2}$ (6)	$2p_{3/2}$ (4)	0.99±0.18	0.94±0.09
In^{114m}	4.1	57±9	5	$1h_{11/2}$	$1g_{7/2}$	$2d_{5/2}$		0.57±0.10	1.23±0.11
	6.2	63±10	5	(2)1.84	(8)7.05	(6)5.35		0.49±0.09	1.33±0.12
I^{126}	4.0	60±15	6	$1h_{11/2}$	$1g_{7/2}$	$2d_{5/2}$		0.86±0.22	1.02±0.13
	6.2	46±11	6	(10)	(8)	(6)		1.06±0.28	0.92±0.13
Ce^{141}	3.0	24±3	10	$2f_{7/2}$ (2)	$2d_{3/2}$ (4)	$3s_{1/2}$ (2)		0.86±0.15	1.00±0.08
La^{141b}	3.0	4.2±0.6	10	$1g_{7/2}$ (8)	$2p_{1/2}$ (2)			2.34±0.39	0.61±0.05
Ta^{180m}	3.0	47±12	4	$1i_{13/2}$	$1h_{9/2}$	$2f_{7/2}$		1.06±0.26	0.92±0.11
	5.7	46±12	47	(8)	(10)	(8)		1.04±0.25	0.92±0.12

[a] The nuclear density distribution parameters, g and r_0, given in this table are partly based on the number of available shells determined from the shell spacings given by Ross, Mark, and Lawson (reference 12) and the highest particle-stable excitation energies of the p,pn products (reference 25). A different nuclear model than the one used by Ross, Mark, and Lawson, would give different shell spacings and consequently different values of g and r_0 than are given here. The spring-constant parameter, g equals $\beta^2/A^{\frac{1}{3}}$, where β is the harmonic-oscillator spring constant. The half-central-density radius parameter, r_0, equals $R/A^{\frac{1}{3}}$, where R is the nuclear radius at which the density is one-half the central value.
[b] $(p,2p)$ product.
[c] Includes $(p,2p)$ cross section.

least-bound particle, an appropriate barrier correction must be added and the sum compared to the neutron binding energy. Except for a very few cases, alpha particles need not be considered. A possible method of computing the barrier correction and the highest particle-stable excitation energies for the p,pn products for which Bev cross sections are available is given elsewhere.[25]

Table II gives the experimental (p,pn)-reaction cross sections and the values of g and r_0 derived from the cross sections, the number of available shells, and values of M_{nl}. Column one gives the (p,pn) product [$(p,2p)$ product in the case of La^{141} and (p,pn) plus $(p,2p)$ product in the case of Mo^{99},Nb^{99}]. Column two gives the proton bombarding energies in Bev at which the cross sections in column three were determined. The cross sections at both 3 to 4 Bev and 5.7 to 6.2 Bev are given, if available, to indicate the spread in the experimental data. Equation (23) was used for the 4-Bev data. The references[1,2,4–6,10,44–47] to the experimental cross-section values are given in column four. Column five gives a possible choice of available shells determined from the eigenvalue calculations of Ross, Mark, and Lawson[12] and the highest particle-stable excitation energies.[25] The target-nucleus neutron-occupation numbers are given in parentheses immediately below each shell. Values of g, derived from the cross sections by the use of Eqs. (18a), (22), or (23), and Figs. 3 or 4, are given in column six. The

[44] N. Horwitz and J. Murray, University of California Radiation Laboratory Report UCRL-8881, August, 1959 (unpublished).
[45] J. B. Cumming, G. Friedlander, and C. E. Swartz, Phys. Rev. **111**, 1386 (1958).
[46] The author wishes to thank Dr. Lester Winsberg for allowing the use of his results before publication.
[47] James Grover, thesis, University of California Radiation Laboratory Report UCRL-3932, September, 1957 (unpublished).

value of r_0, the half-central-density radius parameter, given in column seven for each cross section is the mean of the two values computed from the upper and lower limits of g by the use of Eq. (16).

The appropriate values of M_{nl} were used to compute the g and r_0 values for the $(p,2p)$ products. Because the effect of the coulomb force is completely neglected, the values of g and r_0 (Mo^{99}, Nb^{99}, and La^{141}) are just rough guesses.

The values of g determined for the target In^{115} must be corrected for the fact that the measured (p,pn) cross section refers only to the isomer In^{114m} $(J=5+)$ and does not include contributions from In^{114} $(J=1+)$.[48] This correction can be estimated by adding vectorially the j value of the neutron hole in a given shell, j_1, to the spin of the target nucleus j_2 to get resultant J's between j_1+j_2 and $|j_1-j_2|$. The fraction of each J state which decays to either one or the other of the isomers is roughly determined by assuming the decay to the ground state to proceed by emission of a single gamma ray of the appropriate multipolarity. The lifetimes for such gamma decays are compared by means of published formulas.[49] Under this simplifying assumption, it turns out that, except for the state with a J value midway between the spins of the two isomers, the states decay essentially entirely into one or the other of the isomers. For a given neutron shell, the number of neutrons effective in producing one of the isomers is obtained by weighting each J state by the statistical weight, $2J+1$, and the fraction decaying into the isomer, summing over all allowed J states, and dividing by $\sum_J(2J+1)$. This final fraction is multiplied by the total number of neutrons in the shell. For $In^{115}(p,pn)In^{114m}$, the effective number of neutrons for each available shell was found by taking the ground-state spin of In^{115} to be $9/2+$ (due to a $1g_{9/2}$ proton hole).[48] The effective number of neutrons so obtained for each shell are given in column five, Table II, to the right of the neutron occupation numbers. It is not possible to make such a correction for Ta^{180m} because the spins of the two isomers are not available. Consequently, values of g and r_0, computed as if the only product were Ta^{180m}, represent upper and lower limits respectively.

Figure 7 is a plot of the half-central-density radius parameter, r_0, given in Table II, as a function of the target atomic weight. Points for 3- to 4-Bev and 5.7- to 6.2-Bev bombarding energies are denoted by triangles and circles, respectively. The error limits given on each point are the experimental error limits only. The dashed lines connect half-charge-density radius parameters as given by the electron-scattering results.[30] The solid lines connect a few radius parameters,

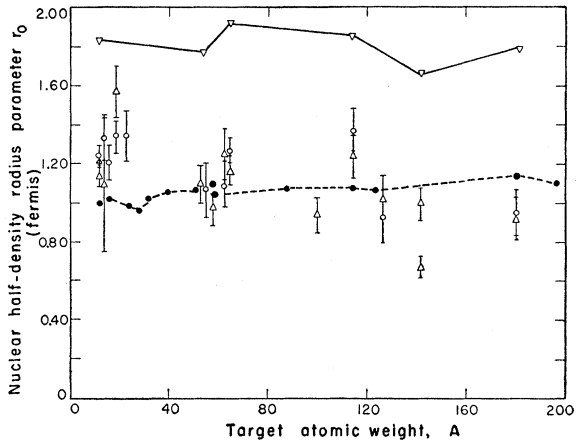

FIG. 7. The half-central-density radius parameter, r_0, as a function of target atomic weight. The points are obtained from experimental 3.0-Bev (△) and 5.7-Bev (○) p,pn-reaction cross sections [Eqs. (22) or (23)], and the static level spacings of Ross, Mark, and Lawson (reference 12). The broken line connects values (●) of r_0 obtained from the electron-scattering results (reference 30). The solid line connects values (▽) of square-density radius parameters, calculated from the formulas in Appendix III, necessary to give the observed p,pn cross sections. These values of r_0 are the ones that would have to be used in the existing Monte Carlo calculations to give agreement between experimental and calculated p,pn cross sections.

r_0, calculated to be necessary to give the observed p,pn cross sections for nuclei containing a degenerate Fermi gas with a uniform density distribution. This is the nuclear model used in the Monte Carlo calculations.[9] The radius parameter, r_0, was calculated from the observed p,pn cross sections at 3 Bev by the use of the equations derived in Appendix III with $\sigma_1=38$ mb and $\bar{\sigma}=150$ mb.

A number of interesting points are revealed on examination of Fig. 7. The very large values of r_0 needed for the uniform-density model (roughly 1.8 fermis) to reproduce the experimental p,pn cross sections, compared with the points for the harmonic-oscillator model and the electron-scattering results (and literature data obtained from total nuclear cross sections[50]) show that the p,pn reaction cross sections cannot be explained without the diffuse nuclear surface. This has already been suspected from the Monte Carlo calculations.[4,9] The values for the half-density radius parameters (0.9 to 1.3 fermis) determined from the harmonic-oscillator well lie fairly close to the half-density radius parameters (1.0 to 1.1 fermis) determined from electron scattering work. Other determinations of nuclear radii give values for r_0 of 1.07 fermis (exponential-well half-density radius parameters)[51] and 1.25 fermis (square density distribution).[52] The agreement between these values of the half-density

[48] D. Strominger, J. M. Hollander, and G. T. Seaborg, Revs. Modern Phys. **30**, 585 (1958).
[49] Stephen Moszkowski, *Beta- and Gamma-Ray Spectroscopy*, edited by K. Siegbahn (Interscience Publishers, Inc., New York, 1955), Chap. XIII.
[50] J. M. Blatt and V. F. Weisskopf, *Theoretical Nuclear Physics* (John Wiley & Sons, Inc., New York, 1952), Chap. IX, pp. 482 to 483, 488 to 492.
[51] Alfred E. Glassgold, Revs. Modern Phys. **30**, 419 (1958).
[52] Sidney Fernbach, Revs. Modern Phys. **30**, 414 (1958).

radii and the values found in this work is quite satisfactory, especially in the light of the discussed uncertainties contributed by the use of the harmonic-oscillator model. It is, of course, not correct to compare half-density radii directly with square-density radii. However, the comparisons made above are rough enough so that errors from this source are relatively small.

Unlike the other nuclei studied in this work, the half-density radius parameters obtained from the p,pn cross sections for C^{12}, N^{14}, and O^{16} can be directly compared with those obtained from the results of the electron scattering from these three nuclei. One reason is that the electron-scattering results were analyzed in terms of a harmonic-oscillator well, as was used here. Another reason is that the available neutron shells are known.[1] Also, as has been discussed, Eqs. (22) and (23) are valid under j-j coupling for C^{12} and O^{16} because they are closed-shell nuclei. The same holds for N^{14} because the one neutron outside the closed shells is the only one available. Still another reason is that the effect of the coulomb force on the nucleon density distribution [Eq. (12)] is small. Finally, there is no numerical error made in using Eq. (16) for C^{12} and O^{16}. This can be shown by substituting the values of $1/\beta$ for C^{12} and O^{16} (given as a_0 in Table I of reference 30) into Eqs. (15) and (16), solving for r_0, and comparing the values so obtained with those given in Table IV, column 8, of reference 30. No electron-scattering data is given for N^{14}, so the value of r_0 for this nucleus is taken to be midway between that of C^{12} and O^{16}.

A direct comparison (see Fig. 7) between the values of r_0 obtained in this work and the electron-scattering work shows that, for C^{12}, N^{14}, and O^{16}, the nucleon half-density radius parameters are larger than the charge half-density radius parameter by 0.1 to 0.5 fermi (exclusive of the 3-Bev N^{14} point because of its large error limit). This difference seems to be somewhat larger than the value of 0.1 ± 0.1 fermi obtained by other means for the differences between the half-nucleon and charge-density radii (the factor of $A^{\frac{1}{3}}$ is included in this latter value).[53] It is difficult to say whether this difference is real or is due to errors in the assumptions used here. Perhaps the zero-degree laboratory scattering-angle approximation or errors inherent in the method of computing $\bar{\sigma}$, as are discussed later, are the cause. It would seem that these error sources are not sufficient to explain this discrepancy. A reduction of r_0 from 1.2 to 1.0 fermis would require an offsetting reduction in $\bar{\sigma}$ from 168 to 80 mb which is quite drastic. The crude method used to estimate the contribution from elastic p-n collisions may also be contributing errors. If F were set equal to 0.9 (the nucleus perfectly transparent to the struck neutron) then $\bar{\sigma}$ would still have to be reduced to 125 mb to give $r_0=1.0$ fermi.

It is interesting to note that, on the basis of the available-shell assignments made, the (p,pn) radius parameters show a decrease with increasing A. Some of the decrease is probably due to the error associated with using Eq. (16). There also appear to be some irregularities associated with major shells; i.e., Fe^{54}, Mn^{55}, and Ni^{58} all have 28 or less protons and a smaller value of r_0 than do Cu^{63}, Cu^{65}, and Zn^{64} (Table II), which have more than 28 protons. Similarly, In^{115}, which has between 28 and 50 protons, has a larger value of r_0 than does I^{127}, Ce^{142}, or Ta^{181} with more than 50 protons. Molybdenum-100 causes some difficulty here, a difficulty which could be resolved by a study of more (p,pn) reactions around mass 100 uncontaminated by $(p,2p)$ reactions. The low-Z elements again show a value of r_0 similar to that of copper, zinc, and indium. Thus it appears as if nuclei with $20<Z<28$ protons and $Z>50$ protons may have smaller half-density radius parameters than the other nuclei. Neutron major shells appear to have less effect, because Mn^{55}, Ni^{58}, Cu^{63}, Cu^{65}, and Zn^{64} all have more than 28 neutrons, and In^{115} and I^{127} have between 50 and 82 neutrons. It must be realized that these ideas regarding shell effects on r_0 are of a *most* tentative nature as they depend on the nuclear model used to determine the values of M_{nl} and which neutron shells are available.

B. Available-Shell and Radius-Parameter Determinations

It is perhaps more profitable to consider both the availability of the shells and the radius parameter as unknowns. Then the (p,pn) cross sections can be used to determine, for each target isotope, values of r_0 as a function of the shells selected to be available. Figure 8 gives values of r_0 as a function of available shells [computed by the use of Eqs. (16), (18a), (22), and (23) and Figs. 3 and 4] for some of the cross sections given in Table II. The ordinate gives the half-density radius parameter, and the abscissa gives the neutron shells in the order in which they appear in the nuclear well.[12,31] The abscissa of each point is the lowest shell considered available: i.e., for that point all shells below are unavailable, and all shells up to and including the highest neutron-containing shell are available. The lines connect points for a given target in the order of the neutron (proton in the case of La^{141}) shell filling in the well.[31] The right-hand point of each series corresponds to only the topmost neutron-containing shell being available. Each series extends to the left to the $1s_{1/2}$ shell (all the neutrons available). However, the series were terminated at a point where the number of shells taken to be available was considered to be more than sufficient for any reasonable nuclear model. The abscissae for the Mo^{99}, Nb^{99} points refer to the lowest

[53] L. Elton, Revs. Modern Phys. **30**, 557 (1958).

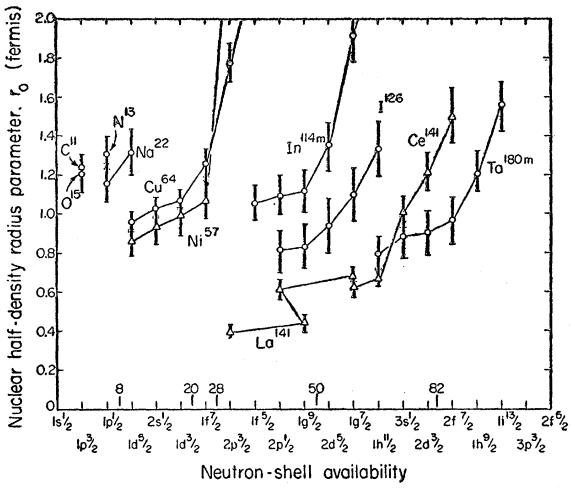

FIG. 8. The half-central-density radius parameter as a function of shell availability. The points are obtained from experimental 3.0-Bev (Δ) and 5.7-Bev (○) p,pn cross sections and Eqs. (22) or (23). The solid lines connect points belonging to the same product. The abscissa of each point gives the lowest shell considered available, i.e., all shells lower down in the potential well are considered unavailable, all the shells higher in the potential well including the highest occupied neutron shell (represented by the right hand point of the series for each product) are considered available. The solid vertical lines of the abscissa represent major neutron-shell closures.

available Mo^{100} neutron shell. The lowest available Mo^{100} proton shell for the first point on the left was taken as $1f_{7/2}$. The rest of the points were computed for a $2p_{3/2}$ proton shell as the lowest available. Several point series, similar to those given, were omitted to avoid clutter. The major neutron shell closures are indicated along the lower margin of Fig. 8.

A point series is given in Fig. 8 for the reaction $Ce^{142}(p,2p)La^{141}$. This has been computed by using neutron wave functions, Eq. (11), for proton wave functions in Eq. (10) and computing values of r_0 as a function of shell availability. (For p-p collisions, σ_1 is about equal to σ_1 for p-n collisions, and the value of $\bar{\sigma}$ should not change much for p-p collisions.)

Except for the points for C, N, and O, Fig. 8 should be considered as only approximately representing the correct situation. Under a coupling scheme any given shell could be partly available, because some of the product parent states with a hole in the given shell may be particle-unstable. Also, the position of the points might be somewhat different if the wave functions corresponding to an inverse exponential well were used. It is to be hoped, though, that the general characteristics of Fig. 8 would be preserved if the correct model were used; accordingly the discussion will be limited to general features.

The series of points for each element all show the same characteristic of a decrease in r_0 as more shells are made available. The steepness of the initial portion on the right of each series is dependent on the number of nucleons in the topmost occupied shell. Iodine-127 and Ta^{181} have many neutrons and protons in their topmost shells, whereas In^{115} has only two neutrons. For several elements, the series of points makes it possible to put lower limits on the number of shells available. Thus for In^{114m} the large value of r_0 required, if only the $1g_{7/2}$ and $1h_{11/2}$ shells are available in In^{115}, make it quite likely that a large part or all of the $2d_{5/2}$ neutron shell is also available. Similarly the unreasonable values of r_0 required for Ni^{57} and Cu^{64} if the $1f_{7/2}$ is unavailable show that much or all of the $1f_{7/2}$ neutron shell is allowed. This is noteworthy in that the $1f_{7/2}$-$1f_{5/2}$ spacing more than crosses a major shell closure. (Mn^{54}, Cu^{62}, and Zn^{63} give the same result.)

If one takes the highest particle-stable excitation energy of the product nucleus into account, upper limits on the excitation energy of populated levels can be set. For example, in the case of In^{114m}, the highest particle-stable excitation energy of 7.0 Mev (neutron binding energy)[25,54] yields the result that most or all of the levels populated by removal of a $2d_{5/2}$ neutron from In^{115} have less than 7.0-Mev excitation energy. Similarly, from the highest particle-stable excitation energy of 7.91 Mev (neutron binding energy[25,55]) for Cu^{64}, one can show that most or all of the Cu^{64} levels populated by removal of a $1f_{7/2}$ neutron from Cu^{65} have an excitation energy less than 7.9 Mev. Similar arguments can be given for Cu^{62}, Zn^{63}, Mn^{54}, and Ni^{57}. Under the independent particle model the above two cases show that the $1h_{11/2}$-$1d_{5/2}$ and $1f_{5/2}$-$1f_{7/2}$ neutron-shell spacings are less than 7.0 and 7.9 Mev, respectively.

These arguments can be carried to other as yet unmeasured (p,pn) cross sections to estimate the energy spacing across other neutron shells. For example for the Nb^{93} or Ru^{96} (p,pn) cross section one can determine the availability of the $1g_{9/2}$ neutron shell and estimate an upper limit for the $2d_{5/2}$-$1g_{9/2}$ shell spacing across the $N=50$ major shell.

C. The Problem of Ce^{142}

Ce^{142} is the only nucleus for which (p,pn) and $(p,2p)$ cross sections are known in the Bev energy region. We see from Fig. 8 that the values of r_0, obtained from the Ce^{141} production cross section, range from less than 0.67 fermi to 1.5 fermis, which is a reasonable range. However, the maximum value of r_0 obtained from the La^{141} production cross section is 0.67 ± 0.05 fermi which is an unreasonably small value. One possible explanation of this low value is that the Coulomb force (which was neglected) concentrates the protons strongly towards the center of the nucleus. This concentration is beyond that already given by the sum over squared harmonic-oscillator wave functions

[54] A. Wapstra, Physica **21**, 367 (1955).

[55] K. Way, R. W. King, C. L. McGinnis, and R. van Lieshout, *Nuclear Level Schemes A=40 to A=92*, Atomic Energy Commission Report TID-5300 (U. S. Government Printing Office, Washington, D. C., 1955), pp. 186, 187.

for $N>Z$ [Eq. (12)]. This seems unlikely, because the concentration required to fit the La^{141} cross section is unreasonably large. Also other work shows that the radial neutron and proton density distributions are not too different from one another.[53,56] Another alternative is that the Ce^{142} nucleus is quite small and has relatively little surface. This also seems unlikely in that a half-density radius parameter of 0.6 to 0.8 fermi is an extreme reduction compared to that for other nuclei. A third alternative is that the order of proton-shell filling in the Ce^{142} well is wrong, and the highest filled proton shell is some shell other than the $1g_{7/2}$ shell with just a few protons in it. However, this alternative is contradicted by the observed ground-state spins and parities of the odd-Z, odd-A nuclei from antimony through lanthanum.[31,48]

Another possible explanation for the small value of r_0 obtained for La^{141} is that there is a strong coupling between the two $2f_{7/2}$ neutrons and the $1g_{7/2}$ proton hole in La^{141}. Therefore many of the La^{141} parent states are unstable to particle emission. This would decrease the number of available neutrons and increase the value of r_0. A similar strong coupling can also be allowed between the two $2f_{7/2}$ neutrons and $1h_{11/2}$, $3s_{1/2}$, and $2d_{3/2}$ neutron-hole states of Ce^{141} if one assumes that the three closely spaced $1h_{11/2}$, $3s_{1/2}$, and $2d_{3/2}$ neutron shells[12] are available. However, the effect of this coupling on La^{141} seems unreasonably large when compared to the effect on other nuclei represented in Fig. 8. It does not seem possible at present to decide between these or any other alternatives as to why the $(p,2p)$ cross section (and r_0) is so low. More Bev $(p,2p)$ cross sections for other elements are definitely needed. This difficulty with cerium will be more thoroughly discussed in a future publication.

D. Nuclear Rearrangement

The approximations used in deriving Eqs. (12) and (21) to (23) and their use with the experimental high-energy (p,pn) cross sections reveal an interesting result. In this work (p,pn) reactions have been assumed to occur when a multi-Bev incident proton enters a nucleus and strikes a neutron in a given shell, and the reaction products leave the nucleus in a time short compared to nuclear rearrangement time. This allows one to consider the nucleus as a container for nucleons whose momenta and shell distribution can be taken to be that of an unperturbed nucleus. After the collision products have escaped, the nucleus is left in any one of a number of excited parent states whose energy distribution is equal to the excitation energy of the neutron-hole state plus the distribution of the rearrangement energy.[57] In this context, the rearrangement energy consists of all the energy released when the nucleus goes from the ground state of the target minus one neutron from a given shell to the corresponding neutron hole states of the product. This energy comes from such sources as the recoupling of the nuclei in open shells when a neutron is removed, a slight radial shrinkage of the nuclear potential well, etc. The point here is that the nuclear rearrangement associated with the snatching of a neutron from an available shell must predominantly populate product states whose rearrangement energy is less than the highest particle-stable excitation energy of the product nucleus, or about 8 Mev. If the rearrangement were such that all populated product states were more than 8 Mev above ground state, all p,pn cross sections would be equal to zero.[57]

It is possible in several cases to set the upper limit on the rearrangement energy associated with the states predominantly populated by nuclear reorganization at less than the highest particle-stable excitation energy of the product nucleus. As has been discussed in another work,[1] the only particle-stable state of N^{13} is the ground state, because the proton binding energy (1.95 Mev) is less than the excitation energy for the first excited state (2.37 Mev).[58] Further, the low value of the (p,pn) cross section for N^{14} is explained satisfactorily by the low number of available neutrons (See Table II and Figs. 7 and 8). Consequently, the nuclear rearrangement associated with the snatching of a $1p_{1/2}$ neutron from N^{14} must predominantly populate the ground state of N^{13}. The energy associated with this rearrangement to the N^{13} ground state must be zero Mev.

A similar situation exists for the product O^{15}. From Table I and Figs. 7 and 8 it can be seen that the $O^{16}(p,pn)O^{15}$ cross section is satisfactorily explained by taking the $1p_{1/2}$ and $1p_{3/2}$ neutron shells to be available. If one assumes that, because of a large rearrangement energy, the $1p_{3/2}$ shell is not available, the half-density radius parameter, r_0, from Eqs. (16), (18a), and (22) and Fig. 3 would have to be 2.1 fermis to give the (p,pn) cross section observed. The large discrepancy between this value and others (see Figs. 7 and 8 and ensuing discussion) supports strongly the availability of the $1p_{3/2}$ shell. The $1p_{3/2}$ neutron-hole state of O^{15} is at 6.14 Mev; there is one more level at 6.86 Mev before the first particle-emitting level at 7.61 Mev is reached.[58] This part of the level scheme shows that the nuclear rearrangement occurring after a $1p_{3/2}$ neutron has been snatched out must predominantly populate either the 6.14-Mev level or the 6.86-Mev level of O^{15}. The respective energies associated with rearrangement to these two levels are zero Mev and 0.68 Mev.

This same argument can be applied to heavier nuclei. It has already been shown how the buried $1f_{7/2}$ neutron

[56] Lawrence Wilets, Revs. Modern Phys. **30**, 542 (1958).

[57] The author is indebted to Professor Ben Mottelson for pointing out this extra source of excitation energy and the fact that it must contribute less energy than the binding energy of the least-bound particle in the product nucleus.

[58] F. Ajzenberg and T. Lauritsen, Revs. Modern Phys. **27**, 77 (1955).

shell in Cu^{63}, Cu^{65}, and Zn^{64} is probably available, because its exclusion gives unreasonably large values of r_0. Snatching a neutron from the $1f_{7/2}$ closed shell of zinc or copper would give a product hole state with appreciable excitation energy (roughly 5 Mev),[12] because it is across both a major and minor (the $2p_{3/2}$) shell. Since the highest particle-stable excitation energy for zinc and copper is 8 to 9 Mev,[25,55] there must be no large population of states whose associated rearrangement energy is greater than 3 to 4 Mev. This figure is quite approximate and is only a rough first guess. This same argument can be applied to other cases such as the $2d_{5/2}$ shell of In^{115} and possibly the $1h_{11/2}$ shell of Ce^{142}. These relationships between simple nuclear reaction cross sections and nuclear rearrangement will be discussed in more detail in a later publication.

Note added in proof.—The ideas expressed in this section regarding nuclear rearrangement and rearrangement energy appear to be consistent with the views expressed by K. Brueckner [Proceedings of the International Conference on the Nuclear Optical Model, The Florida State University, Tallahassee, Florida, March, 1959, Pages 132–144].

E. Other Uses of (p,pn) Cross Sections

We have shown how the p,pn cross section can be used to obtain information about rearrangement energy and shell availability. Here we wish to point out that for some nuclei the high and low angular momentum subgroups of the group of available neutron shells can be studied separately. To do this, one has to measure the (p,pn)-reaction cross sections to two isomeric product states of an even-N-even-Z target nucleus. Because the ground state of such a target has a value of $J=0$, the sudden removal of a neutron will leave the product nucleus in states whose J values are all equal to the j value of the removed neutron. The strong gamma ray lifetime dependence on the multipolarity of the transition strongly weights the populating of the high- and low-spin isomers by the high- and low-angular-momentum neutron shells, respectively. This division of the neutron shells is not nearly so clean-cut for the even-N-odd-Z targets with isomeric product states which are the only ones studied so far. This is because the neutron hole produced by the sudden removal of the neutron can couple with the J value of the target nucleus to give a whole range of spins.

Another possible use of p,pn reaction cross sections can be seen from a closer examination of Eq. (21). Suppose the p,pn reaction cross sections were known for a series of isotopic targets in which a large neutron shell was filling. Then Eq. (21) shows that a plot of $\sigma_{p,pn}$ against the neutron number in the filling shell is an almost straight line (the A dependence of M_{nl} over a restricted A range is small at large A) whose slope equals M_{nl} for the filling shell. In this manner it appears possible in some cases to determine M_{nl} experimentally.

VII. POSSIBLE ERROR SOURCES

It has been shown how the results of the theory embodied in Eqs. (21) to (23) and Figs. 3 and 4 may help to understand nuclear structure more clearly by yielding information about nuclear radii, rearrangement energy, and hole-state excitation energies. These results have been derived from a theory based on several simplifying assumptions, such as the impulse approximation, single nucleon-nucleon collisions, classical nucleon and pion trajectories inside the nucleus, and a very approximate treatment of elastic p-n collisions. Besides these assumptions and the difficulties inherent in using the independent-particle harmonic-oscillator model to represent real nuclei, there are other implicit approximations in the theoretical results. A discussion of these points will help to put this work in a better perspective.

There are a few sources of possible error in the assumption made that the effective average exit cross section, $\bar{\sigma}$, is a sum of exclusion-principle-corrected cross sections for pion-nucleon and nucleon-nucleon collisions averaged over event types and particle energies. One source stems from the neglect of the wave properties of high-energy pions and nucleons. If a nucleon and a pion are scattered at an included angle of 20° and 300-Mev kinetic energy each—which are not unreasonable figures[15,16]—then the nucleon and pion must travel 0.8 and 1.1 fermis respectively before their separation is greater than the pion reduced wavelength. This is an appreciable distance of travel compared to nuclear dimensions. For this part of their paths where the particles are closer than a wavelength apart, the cross section for interaction with nucleons would not be just a sum of individual nucleon-nucleon and pion-nucleon collision cross sections because there would be some sort of interference.

Another source of error which also arises from the neglect of the wave properties of the colliding nucleons is that, depending on the angular distribution of the emitted nucleons and mesons, the momentum transfer to the target nucleon along the incident-particle direction can be very small for high incident energies. The uncertainty principle then shows that it can be impossible to localize the collision to within a nucleon dimension, or even nuclear dimensions as has been done in Eqs. (1) ff. This problem has been treated in the literature and conditions are given to determine if the collisions can be localized.[59] The meson energies in the "reconstructed events" used to determine $\bar{\sigma}$, were used in the appropriate condition equation.[59] It appears that on the whole the picture of a collision localized to within nuclear dimensions has approximate

[59] E. Feinberg, J. Exptl. Theoret. Phys. (U.S.S.R.) **28**, 241 (1955) [translation: Soviet Phys.-JETP **1**, 176 (1955)].

validity. For about one-half of the $pp\pi^-$ events and most of the $pn\pi^+\pi^-$ and $pn\pi^+\pi^-\pi^0$ events at $E_N=3.8\pm2.4$ Bev, the collisions are localized to nucleon dimensions.

An error source affecting $\bar{\sigma}$ may exist if the isobar model of pion production from high-energy nucleons is valid inside the nucleus.[16,35] Since the isobar states have small but finite lifetimes, the nucleon-nucleon collision products traverse the first part of the path as isobars which then each decay into pions and a nucleon. Consequently for the first part of the path, $\bar{\sigma}$ consists of cross sections for nucleon isobar-nucleon collisions. An error is introduced unless these cross sections are equal to the sum of the individual cross sections for collisions between isobar-decay products and nucleons.

The assumption that the pion-nucleon collison cross sections used to determine $\bar{\sigma}$ are the same inside the nucleus as outside may be a further source of error. Recent theoretical work shows that various parameters describing pion interactions inside a nucleus vary strongly with energy.[60] However, the errors made in assuming the free pion-nucleon cross sections to hold inside the nucleus should be small, except possibly near the resonance.[60] The free *n-p* scattering data do not show strong peaking in the produced meson intensity at the resonance energy. For this reason and possible similar hard-to-correct errors in "lifting" the free *n-p* scattering data into the nucleus, no correction was made for this error source.

The magnitude of the error arising from these sources in the approximations used to develop the theory is very difficult to determine. It is hoped that it is small, possibly through cancellation effects of the individual errors. Perhaps in the future it will be possible to evaluate the uncertainties arising from these sources.

There are several small errors arising from the experimental input *p-n* collision data and the methods of handling the data. One uncertainty in the input data is that, for $pn\rightarrow pn\pi^+\pi^-\pi^0$ and other less frequent events, the number of neutral pions produced is uncertain.[16] For this work, the number of π^0 particles in each event type explicitly stated in the input data was used. There is some evidence that the average π^0 multiplicity is somewhat larger than that given by the above data.[18] Several errors arising from the method of treatment of the input data include neglecting the few high meson-multiplicity events in the input data (the five-prong and a few of the three-prong events were neglected) and letting $A/2=N=Z$ for all target nuclei in the determination of $\bar{\sigma}$. These and other errors arising from the method of event reconstruction and estimation of the reduction in $\bar{\sigma}$ due to the exclusion principle should be small.

[60] K. Watson and C. Zemach, Nuovo cimento **10**, 452 (1958); K. Watson (private communication).

VIII. SUMMARY AND CONCLUSION

The failure of the model used in the Monte Carlo calculations to predict either the right magnitude or dependence on target element of the *p,pn* cross sections for Bev protons has been evident for some time. The lack of a nuclear surface and shell structure in the model have been suggested as the most likely reasons for lack of agreement between theory and experiment.

In order to remedy this situation, a theoretical treatment of simple nuclear-reaction cross sections, as exemplified by that of the *p,pn* reaction, was developed. This allows the use of several different nuclear models. The theory is based on several simplifying approximations which appear to be valid in the multi-Bev bombarding-energy range. These approximations include the impulse and zero-degree scattering-angle approximations, use of classical trajectories for the incident and scattered particles, and quantum mechanical treatment of the target particle. Equations (9) and (10) give the results of using the above simplifying approximations in the theoretical treatment.

In order to obtain numerical results, the independent-particle harmonic-oscillator nuclear model with spin-orbit coupling was chosen because it gives a diffuse nuclear surface, shell structure, and analytic wave functions. In the interests of self-consistency, the same wave functions were used to give the total nuclear density as well as the probability of finding a nucleon with a given set of quantum labels at a given point. Equation (13) was integrated on the IBM-701 computer for several shells and target elements over the periodic table for a range of values of the spring constant. The cross sections σ_1 and $\bar{\sigma}$ were set equal to 30 mb and 180 mb, respectively; $\bar{\sigma}$ was estimated from the 3.8-Bev cloud chamber data. Also M_{nl} was determined as a function of $\bar{\sigma}$ and σ_1 for selected shells of F^{19}, Cu^{65}, and Ce^{142}.

The contribution to the *p,pn* reaction cross section from elastic *p-n* collisions was roughly estimated by dividing the energy gain of the struck neutron into 3 regions, 0 to 8 Mev, 8 to 18 Mev and $\geqslant$18 Mev. The first region never contributes, the second always contributes, and one half of the third region was assumed to contribute. It was shown that even with wide error limits on the contributing fraction of the third region, the error limits on r_0 from this source is only 7% for 5.7-Bev bombarding energy.

In order to apply the above results to nuclei, $\bar{\sigma}$ was carefully determined from the 1.7- and 4-Bev neutron cloud chamber data to be 160 mb and 168 mb, respectively. The values of σ_1 were taken to be 33.6 ± 1.6 mb and 38 ± 2 mb at 5.7 and 3.0 Bev, respectively. These values of σ_1 and $\bar{\sigma}$ were included in Eqs. (22) and (23) by means of Eqs. (18b) and (18c).

Experimental values of $\sigma_{p,pn}$ were used in Eqs. (22), (23), (18a), and (16) to give the nuclear half density radius parameters as a function of shell availability.

The use of reasonable choices of shell availability gave values of r_0 which are in satisfactory agreement with those obtained by electron scattering and other types of measurement (Fig. 7). This is in contrast to the model used in the Monte Carlo calculations and confirms the requirement of a diffuse nuclear surface for the explanation of (p,pn) reaction cross sections.

The low-Z elements, for which the available shells are known and the harmonic-oscillator model is valid, give values of the nuclear half-density radius parameter of 1.2 ± 0.1 fermis (Fig. 7), which is larger than the value of 1.03 fermis for the electron-scattering charge distribution using the same nuclear model. It is difficult to say whether this difference is real or whether it is due to errors in the assumptions used in this work. The values of F and $\bar{\sigma}$ would have to be changed rather drastically to bring r_0 down to 1.0 fermi.

The results (Fig. 8) show also how the idea of a reasonable value of the nuclear radius parameter may be used with some (p,pn) cross sections to determine the minimum number of available shells. Coupled with the highest particle-stable excitation energy of the product nucleus, this information can be used to help decide which nuclear models give more appropriate energy eigenvalues. For example, this argument shows that in Zn^{64}, Cu^{63}, and Cu^{65} the $1f_{7/2}$-$1f_{5/2}$ neutron-level spacing must be appreciably less than 8 Mev.

The Ce^{141} and La^{141} data present somewhat of a problem in that the (p,pn) and $(p,2p)$ cross sections are low. One possible explanation is that strong nucleon-nucleon coupling reduces the number of available nucleons for the (p,pn) and $(p,2p)$ reactions. Another possible explanation is that the protons are well inside the neutrons—even farther than is indicated by the fact that N is greater than Z.

A general consideration of the mechanism of (p,pn) reactions at high energies shows that the rearrangement energy associated with states predominantly populated by nuclear reorganization after a neutron has been snatched away must be less than the highest particle-stable excitation energy of the product nucleus (roughly 8 Mev). This upper limit on the rearrangement energy of largely populated states can be extended even lower for several target nuclei. In particular, for N^{14} and O^{16} targets the energy associated with the rearrangement to the N^{13} ground state and the 6.14- and 6.82-Mev states of O^{15} must be zero Mev and less than 0.68 Mev, respectively. A similar conclusion holds for the targets Zn^{64}, Cu^{63}, and Cu^{65} for which it is shown that the buried $1f_{7/2}$ neutron shell is very likely available. The appreciable $1f_{7/2}$ hole-state excitation energy in these targets depresses the upper limit of the rearrangement energy for populous product states well below the highest particle-stable excitation energy.

The existence of isomeric states of the (p,pn) product allows the division of the available shells into high and low angular momentum groups and the separate study of each group. Even-even target nuclei are much more suitable for this purpose than are even-odd nuclei. This is because there is only one spin and parity possible for a neutron hole in a given shell. For even-N, odd-Z targets, a wide range of spins is usually possible for a hole in a given neutron shell.

The results of this work indicate that much information may be obtained from (p,pn)-reaction cross sections in the multi-Bev region. Much more experimental data is certainly needed. Furthermore, all but a small part of this work covered (p,pn) cross sections, whereas $(p,2p)$-, $(p,p\pi^+)$-, and $(p,p\pi^-)$ [or (p,n)]-reaction cross sections can also be treated in the same manner as the (p,pn) cross sections. Equation (10) holds for $(p,2p)$ as well as (p,pn) reactions and, with the inclusion of other factors, can also be used for $(p,p\pi^+)$ and $(p,p\pi^-)$ reactions.

IX. ACKNOWLEDGMENTS

I would like to express my gratitude to Professor I. Perlman under whose supervision this work was done. I want to thank Professor John Rasmussen and Professor Kenneth Watson, Dr. Lester Winsberg and Dr. Jack Uretsky, and especially Dr. Wladyslaw Swiatecki for many helpful and illuminating discussions. I am very grateful to Professor Ben Mottelson for reading this manuscript and offering many helpful suggestions. My thanks are extended to Alice McMullen for assistance with the computer programming. Ted Ross, Tom Dowd, and the computer-center group were very helpful with the IBM-701 computer operation.

APPENDIX I

Angular and energy distributions are easily obtained from elastic p-p collisions, because the angular dependence of the scattered products at high energies in the c.m. system is known.[21,22] In the absence of experimental data at Bev energies, the angular dependence of the p-n elastic cross section in the c.m. system is taken to be the same as that of the p-p elastic cross section in the forward c.m. hemisphere.[61]

For elastic nucleon-nucleon collisions, the recoil energy, T_2, in the laboratory system of the target particle is given by Morrison,[62] Eqs. (7a) and (13):

$$T_2=mc^2[(\gamma-1)/2](1+\cos\theta), \qquad \text{(A1)}$$

[61] The author is indebted to Professor Kenneth Watson for suggesting the following angular dependence, extrapolated from existing experimental data, for elastic collisions of Bev protons incident on neutrons. The proton differential-scattering cross section in the forward c.m. hemisphere can be taken to be the same as that from p-p elastic collision data. This is the forward diffraction peak. Superimposed on this is an isotropic differential-scattering cross section. For p-n collisions, this can be considered equal to the 90° c.m. differential-scattering cross section from elastic p-p collisions. At multi-Bev energies, this differential-scattering cross section is very small (reference 21) and has been neglected by the author.

[62] Philip Morrison, *Experimental Nuclear Physics*, edited by E. Segré (John Wiley & Sons, Inc., New York, 1953), Vol. 2, Part VI, pp. 3 to 11.

where θ is the scattering angle of the *target* nucleon in the c.m. system, and $\gamma-1$ gives the laboratory kinetic energy in units of mc^2. The laboratory scattering angle, θ_2, of the target particle, as given by Eqs. (6) and (13) of reference 62 and a trigonometric identity, is

$$\cos\theta_2=\frac{(\gamma-1)+(\gamma+3)\cos\theta}{(\gamma+3)+(\gamma-1)\cos\theta}. \tag{A2}$$

The number of neutrons from elastic p-n collisions, $(dN/d\theta)d\theta$, scattered per unit scattering c.m. angle into the solid angle $2\pi\sin\theta d\theta$ and normalized to one incident proton, is given by

$$dN/d\theta=(n+1)\cos^n\theta\sin\theta. \tag{A3}$$

This result is obtained from the $\cos^n\theta$ dependence of the p-p differential scattering cross section in the forward c.m. hemispheres.[21]

The fraction of collisions, F_T, which scatter target neutrons with a laboratory recoil kinetic energy of T or less is obtained by integrating Eq. (A3) between the limits π and θ_M. The value of θ_M is obtained from Eq. (A1) with T_2 set equal to T. These operations give

$$F_T=\{1-[1-2T/mc^2(\gamma-1)]^{n+1}\}. \tag{A4}$$

APPENDIX II

Equations (15) and (16) can be derived by considering the nucleus as a degenerate Fermi gas. Then the nucleon density, ρ, is given by[63]

$$\rho=[16\pi(2m)^{\frac{3}{2}}/3h^3]T^{\frac{3}{2}}, \tag{B1}$$

where T is the Fermi kinetic energy of the nucleons, and m is the nucleon mass.

For a harmonic-oscillator nuclear well, T is given by

$$T=T_0-\tfrac{1}{2}m\omega^2r^2, \tag{B2}$$

where T_0 is the Fermi energy at the center of the nucleus and ω is the oscillator frequency. If R_0 is the classical turning point of a nucleon with the Fermi energy [obtained from Eq. (B2) by setting T equal to zero], then from Eqs. (B1) and (B2) we have

$$\rho/\rho_0=(1-r^2/R_0^2)^{\frac{3}{2}}, \tag{B3}$$

where ρ_0 is the central nuclear density. Normalization of Eq. (B3) to require that A nucleons are contained in a sphere of radius R_0 gives

$$\rho_0=8A/\pi^2R_0^3. \tag{B4}$$

Because Eq. (B1) also gives a relation between ρ_0 and T_0, use of Eqs. (B4) and (B2) (at $T=0$) and Eq. (B1) gives

$$\omega=(\tfrac{3}{2})^{\frac{1}{2}}(2A^{\frac{1}{3}}\hbar/mR_0^2). \tag{B5}$$

Since we have[29]

$$\beta=(m\omega/\hbar)^{\frac{1}{2}}, \tag{B6}$$

we obtain

$$\beta^2=(\tfrac{3}{2})^{\frac{1}{2}}(2A^{\frac{1}{3}}/R_0^2). \tag{B7}$$

For use here it is preferable to give β^2 in terms of the half-density radius, R, rather than the turning-point radius. From Eq. (B3) it can be seen that $R^2=R_0^2[1-(\frac{1}{2})^{\frac{2}{3}}]$. Writing $R=r_0A^{\frac{1}{3}}$ and evaluating the numerical constants we finally get

$$\beta^2=0.847/A^{\frac{1}{3}}r_0^2=g/A^{\frac{1}{3}}, \tag{B8}$$

where g is given by

$$g=0.847/r_0^2. \tag{B9}$$

In spite of the approximations involved in using Eq. (B1),[63] Eqs. (B7) and (B8) give fairly accurate values of the half-density radius parameter, r_0. This was checked by plotting the actual nuclear density distribution as a function of the radius for a few values of g by using Eq. (14) and the shell occupation numbers of Mayer and Jensen[31] for three nuclei, F^{19}, Cu^{65}, and Ce^{142}. Table III gives the results. A comparison of the results in Columns 3 and 4 shows that r_0 obtained from Eq. (B8) varies from being 3% too large for F^{19} to 9% too small for Ce^{142} when compared to the correct values of r_0 obtained from Eq. (14).

TABLE III. Comparison of half-density radius parameters.

Element	g (fermis)$^{-2}$	Half-density radius parameter, r_0(fermis) from Eq. (B9)	Half-density radius parameter, r_0(fermis) from Eq. (14) and Mayer and Jensen[a]
F^{19}	0.60	1.19	1.16
	0.80	1.03	1.00
Cu^{65}	0.50	1.30	1.37
	0.80	1.03	1.06
Ce^{142}	0.80	1.03	1.12
	0.90	0.97	1.06

[a] See reference 31.

[63] Wladyslaw Swiatecki, Proc. Phys. Soc. (London) **A68**, 285 (1955). The author is indebted to Dr. Swiatecki for a valuable discussion about the points covered in Appendix II.

APPENDIX III

The (p,pn) cross sections as a function of r_0 for the model of the nucleus used in the Monte Carlo calculations[9] can be computed easily under the assumptions made in this work, since all the necessary integrations can be performed analytically. The nuclear model used for the Monte Carlo calculations was that of a degenerate Fermi gas with a uniform radial density distribution out to $R_0=r_0A^{\frac{1}{3}}$. For R greater than R_0, the density was set equal to zero.

These characteristics can be easily put into Eq. (10) of the main part of this work. Since the radial distribution is independent of the position and momentum of the nucleons, the $_{n,l,j}$ subscript can be removed from $T_{n,l,j}(r^2+z^2)$, and we can write for the normalized single-nucleon distribution

$$T^2=3/r_0^3A, \tag{C1}$$

where the factor of $\frac{1}{2}$ is outside the integrals in Eq. (10). In this model, the two density factors, $\rho(R)$ and $\rho'(R)$ will be set equal to one another because the one nucleon less in $\rho'(R)$ will have even a smaller effect than for the harmonic-oscillator model. Normalization of $\rho(R)$ to contain A nucleons in a sphere of radius $R_0=r_0A^{\frac{1}{3}}$ gives

$$\rho(R)=3/4\pi r_0^3. \tag{C2}$$

Substitution of Eqs. (C1) and (C2) into Eq. (10) and changing the infinite limits to limits on the surface of the sphere gives

$$M=\frac{3}{2r_0^3A}\int_0^{R_0} rdr \int_{-(R_0^2-r^2)^{\frac{1}{2}}}^{(R_0^2-r^2)^{\frac{1}{2}}} \times\exp\left[-\frac{3\sigma_1}{4\pi r_0^3}\int_z^{(R_0^2-r^2)^{\frac{1}{2}}} dy-\frac{3\bar{\sigma}}{4\pi r_0^3}\int_{-(R_0^2-r^2)^{\frac{1}{2}}}^{z} dy\right]dz.$$

Evaluation of the integrals gives

$$M=\frac{8\pi^3r_0^6}{9A(\bar{\sigma}-\sigma_1)}\left[\frac{1-(1+2a_1)\exp(-2a_1)}{\sigma_1^2}-\frac{1-(1+2\bar{a})\exp(-2\bar{a})}{\bar{\sigma}^2}\right], \tag{C3}$$

where

$$a_1=3\sigma_1A^{\frac{1}{3}}/4\pi r_0^2,$$

and

$$\bar{a}=3\bar{\sigma}A^{\frac{1}{3}}/4\pi r_0^2.$$

For $A\gg1$, the sum over the allowed shells in Eqs. (22) and (23) can be replaced by an integral over the Fermi-gas density distribution from the Fermi energy T_F to a depth E_b down from the top of the Fermi sea. Here E_b is the highest particle-stable excitation energy.[25,54] Because M given by Eq. (C3) is independent of the integration variable in Eqs. (22) and (23), it can be moved outside the integration. Then one has

$$n_a=\int_{T_F-E_b}^{T_F}\left(\frac{dn}{dT}\right)dT, \tag{C4}$$

where n_a is the number of allowed neutrons.

The neutron density per unit energy, dn/dT, for a Fermi gas, which is determined from Eq. (B1) of Appendix II,[63] is

$$\frac{dn}{dT}=\frac{4\pi(2m)^{\frac{3}{2}}T^{\frac{1}{2}}}{h^3}\left(\frac{4\pi r_0^3A}{3}\right), \tag{C5}$$

where the last factor on the right converts $d\rho/dT$ into dn/dT. The fermi energy is obtained from Eq. (C5) by the requirement that

$$\int_0^{T_F}(dn/dT)dT=N,$$

where N is the total number of neutrons in the nucleus. Substitution of Eq. (C5) into Eq. (C4) along with the normalization condition for T_F gives, after rearrangement,

$$n_a=N\left\{1-\left[1-\frac{32mr_0^2E_b}{h^2}\left(\frac{\pi^2A}{18N}\right)^{\frac{2}{3}}\right]^{\frac{3}{2}}\right\}. \tag{C6}$$

Equations (22) and (23) give

$$\sigma_{p,pn}=\sigma n_aM, \tag{C7}$$

where $\sigma=36$ mb for 3-Bev protons and 34 mb for 5.7-Bev protons. The substitution of Eqs. (C6), (C3), and (C4) into Eq. (C7) allows one to find what values of r_0 are necessary to give the observed (p,pn) cross sections for different target elements. As before, σ_1 for 3- and 5.7-Bev protons is 38 ± 2 mb and 33.6 ± 1.6 mb, respectively. The value of $\bar{\sigma}$ was determined in the same manner as before except for $T_F=20$ Mev and was found to be 150 mb for 4-Bev neutrons on hydrogen. If r_0 is set equal to 1.3 fermis, as was done in the Monte Carlo calculations,[9] $\sigma_{p,pn}$ from Eq. (C7) for 3-Bev protons on Cu^{65} and Ce^{140} turns out to be 5.3 mb and 5.7 mb, respectively. These values are in satisfactory agreement with the actual Monte Carlo calculations which give values of $\sigma_{p,pn}$ for 1.8-Bev protons on Cu^{64} and Ce^{140} of 7 ± 3 mb and 10 ± 5 mb, respectively.[4]